Supporting Information for:

Triperyleno[3,3,3]propellane triimides: Achieving a New Generation of Quasi-D_{3h} Symmetric Nanostructures in Organic Electronics

Lingling Lv,[a] Josiah Roberts,[b] Chengyi Xiao,[a] Zhenmei Jia,[a] Wei Jiang,[a] Guowei Zhang,[a] Chad Risko, *[b] and Lei Zhang *[a]

[a] Beijing Advanced Innovation Center for Soft Matter Science and Engineering, Beijing University of Chemical Technology, Beijing 100029, P. R. China

[b] Department of Chemistry & Center for Applied Energy Research, University of Kentucky, Lexington, Kentucky 40506-0055, United States

Table of contents

1. **Materials and methods.....S2**
2. **Synthesis and characterization of compounds.....S2**
3. **CV and UV spectra of the compounds.....S5**
4. **X-ray crystallographic data for compounds.....S5**
5. **Additional DFT data.....S6**
6. **OFET fabrication and characterization.....S14**
7. **References.....S16**
8. **^{1}H NMR, ^{13}C NMR, and HRMS spectra of compounds.....S17**
9. **HMBC and 1D NOE spectra of compounds.....S31**

1. Materials and methods:

All chemicals were purchased from commercial suppliers and used without further purification unless otherwise specified. THF was freshly distilled prior to use. Compounds **1** and **2** were synthesized according to the literature.[1]

^{1}H NMR and ^{13}C NMR spectra were recorded in deuterated solvents on Bruker ADVANCE 400 NMR Spectrometer and Bruker FOURIER 100 NMR Spectrometer. Mass spectra (MALDI-TOF-MS) were determined on a Bruker BIFLEX III Mass Spectrometer. High resolution mass spectra (HRMS) were determined on Bruker Apex IV Fourier Transform Mass Spectrometer.

2. Synthesis and characterization of compounds

Compound 3

Compound **2** (2.2 g, 3.44 mmol) and bis(pinacolato)diboron (3.15 g, 12.39 mmol) were dissolved in anhydrous DMF (50 mL) in a two-neck round bottomed flask. Potassium acetate (0.28 g, 30.98 mmol) and Pd(dppf)Cl_2 (0.13 g, 0.17 mmol) were then quickly added into the flask. The resulting mixture was vigorously stirred under nitrogen and heated at 90 ^{o}C for 24 hours. After cooling, the precipitate was collected by filtration and washed with methanol to give the compound **3** (1.97 g, 75 %) as a white power. ^{1}H NMR (400 MHz, $CDCl_3$, 300 K): δ = 8.38 (d, *J* = 8.2 Hz, 3H), 8.11 (dd, *J* = 7.3, 2.5 Hz, 3H), 8.01 (d, *J* = 7.4 Hz, 6H), 7.56 (t, *J* = 7.7 Hz, 3H), 1.33 (s, 36H); ^{13}C NMR (126 MHz, CD_2Cl_4, 373K): δ = 150.98, 150.68, 150.39, 147.67, 147.37, 147.08, 138.88, 137.62, 137.19, 132.50, 130.55, 129.60, 129.52, 126.97, 126.82, 126.73, 126.63, 120.75, 119.90, 119.51, 84.36, 25.70; HR-MALDI-TOF (m/z): calcd. for $C_{50}H_{51}B_3O_6$: 780.3982; found 780.3957.

Compound 4

A mixture of **3** (1.2 g, 1.54 mmol), 4-bromo-1,8-naphthalic anhydride (1.53 g, 5.55 mmol), EtOH (18 ml), and 2 M Na_2CO_3 (6 ml) in toluene (120 ml), was stirred vigorously and heated to reflux for 24 h. After cooling, the white precipitate was collected and washed with methanol, acetone, THF, and hot toluene to give **4** as a white powder (1.37 g, 90 %). The crude product was used in the next step without further purification. HR-MALDI-TOF (m/z): calcd. for $C_{68}H_{30}O_9$:990.1895, found:990.1894.

Compound 5

To a solution of **4** (2.6 g, 2.63 mmol) in *o*-dichlorobenzene (50 ml), $AlCl_3$ (11 g, 78.77 mmol) was added. The resulting mixture was heated to 175 ^{o}C for 12 hours under nitrogen. After cooling, the resulting solution was added to 2 M HCl (200 ml) and stirred for another 2 h. The crude product was filtrated and washed with methanol, THF and hot tolene to give **5** (1.5 g, 30%) as a black red solid. HR-MALDI-TOF (m/z): calcd. for $C_{68}H_{24}O_9$:984.1426, found:984.1434.

Compound 6

A mixture of compound **5** (1.51 nmol) and amine (16 mmol) were dissolved in anhydrous DMF (50 mL) in a two-neck round bottomed flask. The resulting mixture was stirred vigorously and heated to 120 ^{o}C for 24 hours. After cooling, the reaction mixture was poured into water and extracted with DCM and dried by anhydrous Na_2SO_4. After the solvent was removed by vacuum, the resulting residue was purified by silica gel column to give **6** as a red solid (100 mg, 22%). ^{1}H NMR (400 MHz, $CDCl_3$, 300 K) δ = 8.51 (s, 6H), 8.41 (d, J = 7.7 Hz, 6H), 8.26 (d, J = 8.1 Hz, 6H), 8.21 (d, J = 7.7 Hz, 6H),

5.20 - 5.13 (m, 3H), 2.27 - 2.17 (m, 6H), 1.87 - 1.77 (m, 6H), 1.37 - 1.17 (m, 36H), 0.83 - 0.76 (m, 18H); ^{13}C NMR (126 MHz, $C_2D_2Cl_4$, 373K): δ = 164.98, 147.15, 138.61, 136.54, 132.07, 131.08, 129.63, 128.23, 128.08, 125.93, 122.97, 121.96, 120.89, 82.09, 55.49, 33.37, 32.48, 27.42, 23.17, 14.54.; HR-MALDI-TOF (m/z): calcd. for $C_{101}H_{93}N_3O_6$: 1443.7070; found, 1443.7077.

Compound 7

To a solution of compound **6** (0.069 mmol) in $CHCl_3$, Br_2 (1.33 g, 8.31 mmol) was added. The resulting solution was stirred at 65 °C for 12 h. After cooling, the reaction mixture was poured into water and extracted with DCM and dried by anhydrous Na_2SO_4. After the solvent was removed by vacuum, the resulting residue was purified by silica gel column to give **7** as a dark purple solid (59.34 mg, 45%). ^{1}H NMR (500 MHz, $C_2D_2Cl_4$, 373 K) δ = 9.77 (d, *J* = 8.0 Hz, 6H), 8.89 (s, 6H), 8.43 (d, *J* = 8.0 Hz, 6H), 5.18 - 5.12 (m, 3H) 2.28 - 2.20 (m, 6H), 1.97 - 1.89 (m, 6H), 1.40 - 1.31 (m, 36H), 0.94 - 0.87 (m, 18H); ^{13}C NMR (126 MHz, $C_2D_2Cl_4$, 373K): δ = 163.62, 147.52, 139.07, 137.23, 134.81, 132.55, 131.81, 130.03, 128.10, 127.84, 122.34, 120.88, 119.51, 81.95, 56.06, 33.26, 32.42, 30.37, 27.35, 23.12, 14.53; HR-MALDI-TOF (m/z): calcd. for $C_{101}H_{87}Br_6N_3O_6$: 1911.1717; found, 1911.1700.

Compound 8

A mixture of **7 (**0.04 mmol), 4-*tert*-Butylphenylboronic acid (65.23 mg,0.37 mmol), $Pd(PPh_3)_4$ (13.85 mg, 0.01 mmol), and 2M Na_2CO_3 in THF, was degassed with argon for 15 min and then heated to reflux for 12 h. After cooling, the organic layer was separated, dried with Na_2SO_4, and purified by silica gel column to afford **8** as a purple solid (52.78 mg, 59 %). ^{1}H NMR (500 MHz, $C_2D_2Cl_4$, 373 K) δ = 8.41 (s, 6H), 7.80 (d, *J* = 8.1 Hz, 6H), 7.56 (d, *J* = 8.1 Hz, 12H), 7.40 (dd, *J* = 7.8, 5.4 Hz, 18H), 5.18 - 5.14 (m, 3H), 2.28 - 2.21 (m, 6H), 1.93 - 1.88 (m, 6H), 1.53 (s, 54H), 1.38 - 1.30 (m, 36H), 0.93 - 0.87 (m, 18H); ^{13}C NMR (126 MHz, $C_2D_2Cl_4$, 373K): δ = 165.15, 152.14, 146.54, 141.94, 139.61, 137.67, 136.31, 134.86, 132.48, 131.27, 130.37, 129.33, 128.98, 127.51, 121.47, 120.36, 55.47, 35.45, 33.35, 32.47, 32.26, 27.39, 23.15, 14.55; HR-MALDI-TOF (m/z): calcd. for $C_{161}H_{165}N_3O_6$: 2236.2704; found, 2236.2717.

Compound 9

Compound **8** (0.04 mmol), I_2 (45.72mg, 0.36mmol) and toluene (80 ml) were added to a standard photocyclization glassware. The mixture was illuminated by Blue light (460-465 nm) for 12 h. The toluene was removed under reduced vacuum and the resulting residue was purified by silica gel column, to afford **9** as a yellow solid (66.72 mg, 75%). ^{1}H NMR (500 MHz, $C_2D_2Cl_4$, 373 K) δ = 10.98 (s, 6H), 10.57 (s, 6H), 10.04(s, 6H), 9.58 (d, J = 8.8 Hz, 6H), 8.38 (d, J = 8.6 Hz, 6H), 5.51 - 5.44 (m, 3H), 2.47 - 2.37 (m, 6H), 2.09 - 1.82 (m, 60H), 1.54 - 1.39 (m, 36H), 0.88 - 0.79 (m, 18H); ^{13}C NMR (126 MHz, $C_2D_2Cl_4$, 373 K): δ = 166.38, 152.24, 147.07, 134.79, 133.12, 130.52, 129.05, 127.49, 127.08, 126.63, 125.87, 125.68, 125.63, 124.69, 124.26, 122.58, 122.09, 120.21, 116.32, 56.02, 36.52, 33.64, 33.09, 32.54, 30.37, 27.56, 23.16, 14.53; HR-MALDI-TOF (m/z): calcd. for $C_{161}H_{153}N_3O_6$: 2224.1765; found, 2224.1754.

Compound 10

A mixture of **7** (0.04 mmol), CuI (2.32 mg, 0.012 mmol), $Pd(PPh_3)_4$ (11.59 mg, 0.01 mmol), and 2-Trimethyltin-5-triisopropylsilyl thiophene (147 mg, 0.37 mmol) in anhydrous toluene (20 mL), was refluxed for 12 h under nitrogen. After cooling, the solvent was evaporated under vacuum and the resulting residue was purified by column to afford **10** as a purple solid (42.51 mg, 37 %). ^{1}H NMR (500 MHz, $C_2D_2Cl_4$, 373 K) δ = 8.58 (s, 6H), 7.85 (d, *J* = 8.2 Hz, 6H), 7.53 - 7.42 (m, 12H), 7.35 (d, *J* = 3.3 Hz, 6H), 5.21 - 5.15 (m, 3H), 2.29 - 2.21 (m, 6H), 1.97 - 1.90 (m, 6H), 1.50 - 1.46 (m, 18H), 1.39 - 1.34 (m, 36H), 1.33 - 1.28 (m, 108H), 0.93 - 0.89 (m, 18H); ^{13}C NMR (126 MHz, $C_2D_2Cl_4$, 373

K) δ = 164.93, 151.17, 146.88, 137.86, 137.74, 137.38, 136.67, 136.41, 132.66, 132.05, 131.10, 130.17, 129.94, 128.66, 128.55, 121.43, 120.35, 55.67, 33.38, 32.49, 30.37, 27.43, 23.14, 19.74, 19.57, 14.55, 13.24, 12.97, 12.87, 12.77; HR-MALDI-TOF (m/z): calcd. for $C_{179}H_{225}N_3O_6S_6Si_6$: 2872.4339; found, 2872.4326.

Compound 11

Compound **10** (0.04 mmol), I_2 (45.72mg, 0.36mmol) and toluene (80 ml) were added to a standard photocyclization glassware. The mixture was illuminated by Blue light (460-465 nm) for 12 h. The toluene was removed under reduced vacuum and the resulting residue was purified by silica gel column, to afford **11** as a yellow solid (85.81 mg, 75%). ^{1}H NMR (500 MHz, $C_2D_2Cl_4$, 373 K) δ = 10.53 (s, 6H), 10.21 (s, 6H), 9.28 (s, 6H), 5.50 - 5.47 (m, 3H), 2.48 - 2.44 (m, 6H), 2.13 - 2.08 (m, 6H), 1.92 - 1.88 (m, 18H), 1.60 - 1.57(m, 108H), 1.40 - 1.34 (m, 36H), 0.88 - 0.85 (m, 18H); ^{13}C NMR (126 MHz, $C_2D_2Cl_4$, 373K): δ = 166.20, 146.87, 144.20, 140.34, 138.30, 133.32, 131.18, 130.87, 127.28, 124.92, 124.72, 124.60, 123.87, 123.68, 122.34, 121.20, 117.07, 56.16, 33.64, 32.53, 30.37, 27.54, 23.16, 19.87, 19.24, 14.53, 13.30; HR-MALDI-TOF (m/z): calcd. for $C_{179}H_{213}N_3O_6S_6Si_6$: 2860.3400; found, 2860.3386.

Compound 12

A mixture of **7 (**0.04 mmol), $Pd(PPh_3)_4$ (11.59 mg, 0.01 mmol), and CuI (2.32 mg, 0.01 mmol) in THF/triethylamine (v:v=1:1), was stirred at room temperature under nitrogen. After 30 mins, 1-octyne (69.2 mg, 0.62 mmol) was added and the resulting mixture was stirred at 80 ^{o}C for 18 h. After cooling, the mixture was poured into 2M HCl and extracted with dichloromethane and dried by anhydrous Na_2SO_4. The solvent was evaporated under vacuum and the crude product was purified by column chromatography (petroleum ether/CH_2Cl_2=1:2 v/v) to afford **12** as a purple solid (47.70 mg, 57 %). ^{1}H NMR (500 MHz, $C_2D_2Cl_4$, 373 K) δ = 10.35 (d, *J* = 8.0 Hz, 6H), 8.71 (s, 6H), 8.36 (d, *J* = 8.1 Hz, 6H), 5.19 - 5.14 (m, 3H), 2.81 - 2.75 (m, 12H), 2.28 - 2.22 (m, 6H), 1.95 - 1.90 (m, 18H), 1.75 - 1.70 (m, 12H), 1.60 - 1.53 (m, 24H), 1.37 - 1.33 (m, 36H), 1.11 - 1.05 (m, 18H), 0.92 - 0.87 (m, 18H); ^{13}C NMR (126 MHz, $C_2D_2Cl_4$, 373K): δ = 164.56, 147.71, 139.21, 137.60, 136.19, 130.23, 129.89, 129.38, 129.30, 128.55, 121.51, 121.03, 119.36, 100.57, 84.15, 55.63, 33.31, 32.46, 32.23, 30.37, 29.67, 29.34, 27.36, 23.32, 23.14, 21.11, 14.71, 14.54; HR-MALDI-TOF (m/z): calcd. for $C_{149}H_{165}N_3O_6$: 2092.2704; found, 2092.2714.

Compound 13

To a solution of **12** (0.04 mmol) in toluene (15 ml), DBU (1.22 mg, 0.008 mmol) was added by a syringe. The resulting mixture was stirred at 110 ^{o}C for 2 days under nitrogen. After cooling, the solvent was evaporated under vacuum and the resulting residue was purified by column chromatography to afford **13** as a yellow solid (20.92 mg, 25 %). ^{1}H NMR (500 MHz, $C_2D_2Cl_4$, 373 K) δ = 10.47 (s, 6H), 9.90 (s, 6H), 9.04 (s, 6H), 5.50 - 5.44 (m, 3H), 4.28 (t, *J* = 7.6 Hz, 12H), 2.50 - 2.43 (m, 12H), 2.50 - 2.43 (m, 6H), 2.14 - 2.07 (m, 6H), 1.99 - 2.06 (m, 12H), 1.78 - 1.85 (m, 12H), 1.67 - 1.61 (m, 12H), 1.42 - 1.31 (m, 36H), 1.11 (t, *J* = 7.3 Hz, 18H), 0.88 (t, *J* = 7.2 Hz, 18H); ^{13}C NMR (126 MHz, $C_2D_2Cl_4$, 373K): δ = 166.57, 146.73, 140.51, 133.49, 133.44, 130.32, 128.90, 128.49, 124.00, 123.92, 122.96, 122.77, 122.13, 121.95, 117.11, 87.70, 55.93, 35.44, 33.66, 32.80, 32.55, 32.34, 30.62, 30.38, 27.55, 23.53, 23.17, 14.73, 14.53; HR-MALDI-TOF (m/z): calcd. for $C_{149}H_{165}N_3O_6$: 2092.2704; found, 2092.2695.

3. CV and UV spectra of compounds

Cyclic voltammetry (CV) and differential pulse voltammetry (DPV) were recorded on a 1000B model electrochemical workstation using glassy carbon discs as the working electrode, Pt wire as the counter electrode, Ag/Ag^+ electrode as the reference electrode, and ferrocene/ferrocenium as an internal potential marker. 0.1 M tetrabutylammonium hexafluorophosphate ($TBAPF_6$) dissolved in dichloromethane was employed as the supporting electrolyte. UV-vis absorption spectra were measured with Hitachi (model U-3010) UV-Vis spectrophotometer.

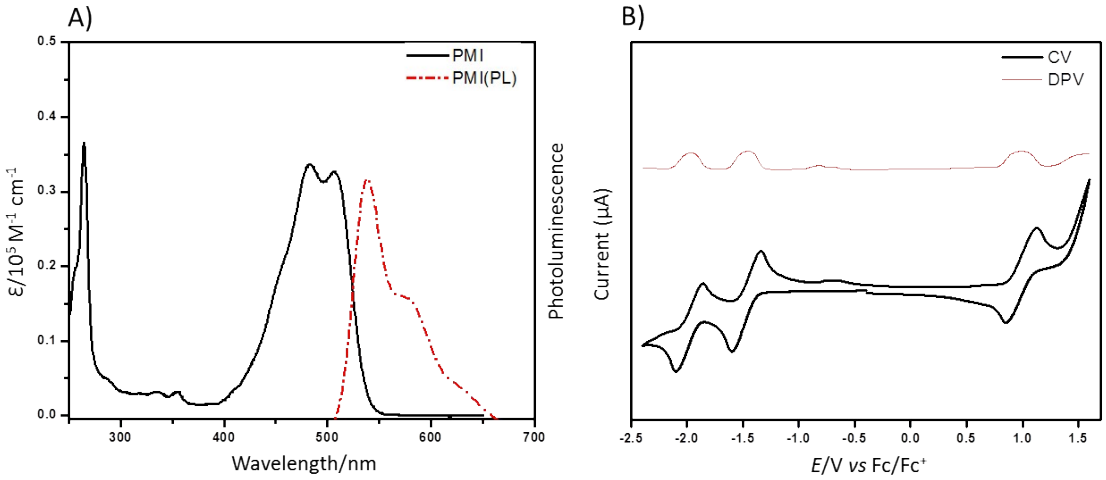

Figure S1. A) UV/Vis absorption (solid line) and photoluminescence spectra (dotted line) of PMI in chloroform (~10^{-5} M), and B) cyclic voltammogram and differential pulse voltammetry (DPV) of PMI. The experiments were performed in nitrogen-purged DCM with tetrabutylammonium hexafluorophosphate ($TBAPF_6$, 0.1 M) as the supporting electrolyte with a scan of 100 mv/s.

4. X-ray crystallographic data for 9

The measurement was made with Synchrotron Radiation (λ = 0.82653 Å). All calculations were performed using the SHELXL-97 and the Crystal Structure crystallographic software package.

Table S1. Crystal data and structure refinement for **9** (CCDC 1894754).

Identification code	**9**	
Empirical formula	$C_{161}H_{153}N_3O_6$	
Formula weight	2225.86	
Temperature	293(2) K	
Wavelength	0.71073 Å	
Crystal system	Monoclinic	
Space group	P2(1)/c	
Unit cell dimensions	a = 18.204(4) Å	α= 90°
	b = 24.592(5) Å	β= 89.882°
	c = 36.283(7) Å	γ = 90°
Volume	16243(6) $Å^3$	
Z	4	

Density (calculated)	0.910 Mg/m^3
Absorption coefficient	0.054 mm^{-1}
F(000)	4752
Crystal size	0.14x 0.07 x 0.04 mm^3
Theta range for data collection	1.00 to 25.02 °
Index ranges	-21<=h<=0, -29<=k<=29, -43<=l<=43
Reflections collected	51162
Independent reflections	27821[R(int) = 0.0448]
Completeness to theta = 25.02 °	97.0 %
Absorption correction	Semi-empirical from equivalents
Max. and min. transmission	0.9978 and 0.9925
Refinement method	Full-matrix least-squares on F^2
Data / restraints / parameters	27821 / 30 / 1733
Goodness-of-fit on F^2	1.601
Final R indices [I>2sigma(I)]	R1 = 0.1249, wR2 = 0.3179
R indices (all data)	R1 = 0.1596, wR2 = 0.3450
Largest diff. peak and hole	1.205 and -0.785 $e.Å^{-3}$

5. Additional DFT data

The electronic, redox, and optical properties of the molecular systems were carried out at via density functional theory (DFT) calculations at the OT-ωB97X-D/6-31g(d,p)[2-4] [OT = optimally tuned] level of theory, where the range-separation parameters ω for each molecule were tuned via the gap-tuning procedure (Table S1).[5-8] Calculations were carried out on the four full molecules (**6**, **9**, **11**, **13**) and on each of the four monomeric units (which we refer to with the superscript "m", i.e. $\mathbf{6}^m$, $\mathbf{9}^m$, $\mathbf{11}^m$, $\mathbf{13}^m$); the aliphatic sidechains in all DFT calculations were truncated to methyl groups to reduce the computational cost. For the monomeric units, the carbon atoms that comprise the joints in the full molecules were terminated with hydrogen atoms to maintain their sp^3 character. We note two aspects pertaining to the level of calculations chosen for these molecules: First, non-empirically tuned long-range corrected density functionals have been shown to describe well the degree of wavefunction and/or charge (de)localization in molecules that may possess mixed-valence character,[9] a potential characteristic of these 3D molecules when oxidized or reduced. Second, the tuned ω parameters provide a first measure of the expected degree of π conjugation / wavefunction (de)localization in the systems.[5-8,10] The ω parameters for the monomers fall within a small range from 0.134 to 0.161; likewise, the ω parameters for the full molecules are quite similar, going from 0.100 to 0.113. Importantly, the smaller ω values for the full molecules suggest an extended wavefunction delocalization when compared to the monomers, even though the monomers are joined by sp^3 carbon atoms in the 3D structures.

The highest-occupied molecular orbitals (HOMO) in $\mathbf{9}^m$, $\mathbf{11}^m$, and $\mathbf{13}^m$ spread over the aryl units appended at the bay positions of $\mathbf{6}^m$, and can be described as linear combinations of the HOMO of the PDI and individual acene moieties (naphthalene in $\mathbf{13}^m$, pentacene $\mathbf{9}^m$, and anthradithiophene in $\mathbf{11}^m$)

that comprise the structures. The lowest-unoccupied MO (LUMO) are likewise combinations of sub-unit LUMO (Figure S3). These variations in chemistry do perturb the HOMO and LUMO energies of **9**^{m}, **11**^{m}, and **13**^{m} when compared to **6**^{m}, with the variations largest for **13**^{m} (Table S1). Notably, the monomers do dis-play some of these wavefunctions delocalized onto the terminal sp^3 carbons.

Table S2. Gap-tuned ω parameters, and adiabatic ionization potentials and electron affinities (AIP and AEA, respectively), and select frontier molecular orbital energies as determined at the OT-ωB97X-D/6-31g(d,p) level of theory.

E (eV)	**6**^{m}	**9**^{m}	**11**^{m}	**13**^{m}	**6**	**9**	**11**	**13**
ω	0.161	0.134	0.138	0.154	0.113	0.0955	0.0969	0.109
IP	6.68	6.52	6.64	6.97	6.57	6.37	6.48	6.80
EA	-1.37	-1.21	-1.13	-0.99	-1.99	-1.69	-1.62	-1.52
LUMO+2	-	-	-	-	-1.60	-1.40	-1.34	-1.22
LUMO+1	-	-	-	-	-1.91	-1.65	-1.58	-1.47
LUMO	-1.23	-1.10	-1.01	-0.86	-1.91	-1.65	-1.58	-1.47
HOMO	-6.79	-6.60	-6.72	-7.06	-6.62	-6.42	-6.53	-6.87
HOMO-1	-	-	-	-	-6.96	-6.70	-6.78	-7.07
HOMO-2	-	-	-	-	-6.96	-6.70	-6.82	-7.14

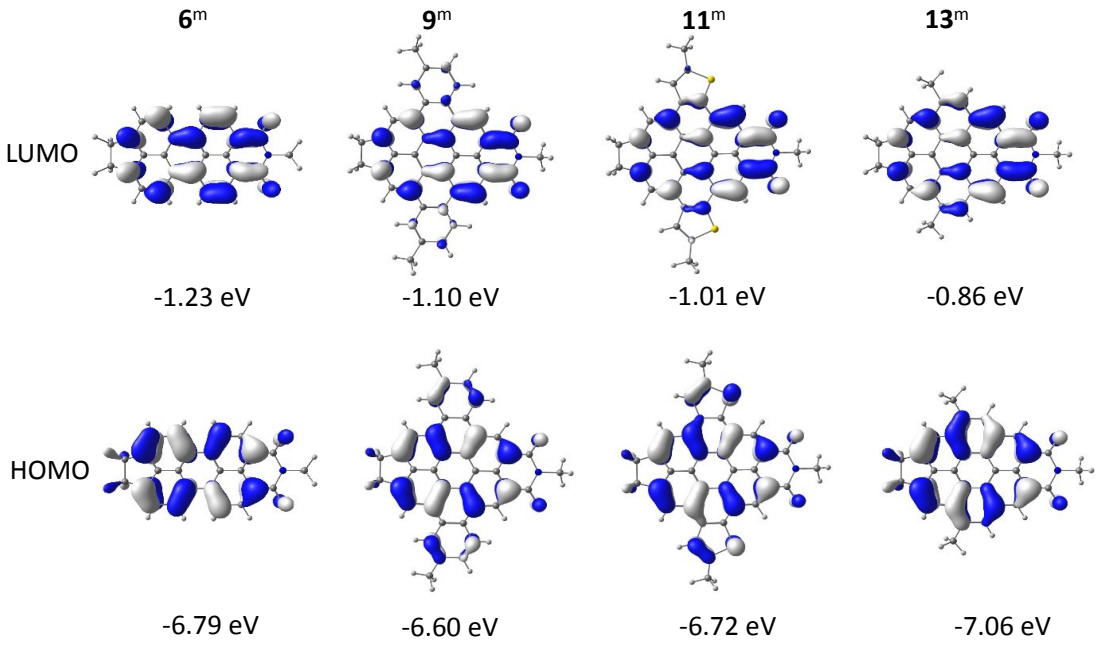

Figure S2. Pictorial representations of select frontier molecular orbitals of the monomer units as determined at the OT-ωB97X-D/6-31g(d,p) level of theory.

Table S3. Select excited-state characteristics for each molecule as determined via TDDFT at the OT-ωB97X-D/6- 31g(d,p) level of theory.

Name	Transition	Energy (eV)	Wavelength (nm)	*f*	Electronic Configuration
6^{m}	$S_0 \rightarrow S_1$	2.86	434	0.68	HOMO → LUMO (98%)

6	$S_0 \rightarrow S_1$	2.56	484	1.25	HOMO - 2 → LUMO (7%) HOMO - 1 → LUMO + 2 (12%) HOMO → LUMO (14%) HOMO → LUMO + 1 (50%)
	$S_0 \rightarrow S_2$	2.56	484	1.25	HOMO - 2 → LUMO + 1 (7%) HOMO - 2 → LUMO + 2 (12%) HOMO → LUMO (50%) HOMO → LUMO + 1 (14%)
9^m	$S_0 \rightarrow S_1$	3.00	413	0.35	HOMO → LUMO (94%)
	$S_0 \rightarrow S_4$	4.01	309	1.13	HOMO - 1 → LUMO (27%) HOMO → LUMO + 1 (60%)
	$S_0 \rightarrow S_9$	4.37	284	0.33	HOMO - 1 → LUMO + 1 (52%) HOMO → LUMO + 4 (33%)
9	$S_0 \rightarrow S_1$	2.50	496	0.71	HOMO → LUMO (83%)
	$S_0 \rightarrow S_2$	2.77	448	0.74	HOMO - 2 → LUMO + 2 (17%) HOMO - 1 → LUMO + 1 (29%) HOMO → LUMO +1 (42%)
11^m	$S_0 \rightarrow S_2$	3.14	395	0.24	HOMO → LUMO (87%)
	$S_0 \rightarrow S_3$	3.89	319	0.99	HOMO - 1 → LUMO (24%) HOMO → LUMO + 1 (69%)
	$S_0 \rightarrow S_4$	3.99	311	0.27	HOMO - 2 → LUMO (29%) HOMO - 1 → LUMO + 1 (50%) HOMO → LUMO (7%)
	$S_0 \rightarrow S_7$	4.17	297	0.33	HOMO - 2 → LUMO (35%) HOMO - 1 → LUMO + 1 (35%) HOMO → LUMO + 4 (9%)
11	$S_0 \rightarrow S_3$	2.91	426	0.59	HOMO - 3 → LUMO + 2 (11%) HOMO - 2 → LUMO (8%) HOMO → LUMO (46%) HOMO → LUMO + 1 (9%)
	$S_0 \rightarrow S_4$	2.91	426	0.58	HOMO - 3 → LUMO (8%) HOMO - 2 → LUMO + 1 (8%) HOMO - 2 → LUMO + 2 (11%) HOMO → LUMO + 1 (47%)
	$S_0 \rightarrow S_5$	2.93	423	0.13	HOMO - 5 → LUMO (28%) HOMO - 4 → LUMO + 1 (28%) HOMO - 1 → LUMO + 2 (19%) HOMO → LUMO + 5 (8%)
13^m	$S_0 \rightarrow S_2$	3.43	362	0.21	HOMO → LUMO (80%)
	$S_0 \rightarrow S_3$	4.18	297	0.50	HOMO - 1 → LUMO (24%) HOMO → LUMO + 1 (62%)
	$S_0 \rightarrow S_5$	4.29	289	0.86	HOMO - 2 → LUMO (9%) HOMO - 1 → LUMO + 1 (70%) HOMO → LUMO (14%)

13	$S_0 \rightarrow S_4$	3.20	387	0.60	HOMO - 5 → LUMO + 1 (9%) HOMO - 5 → LUMO + 2 (11%) HOMO - 4 → LUMO (9%) HOMO → LUMO (54%)
	$S_0 \rightarrow S_5$	3.20	387	0.60	HOMO - 5 → LUMO (9%) HOMO - 4 → LUMO + 1 (9%) HOMO - 4 → LUMO + 2 (11%) HOMO → LUMO +1 (54%)
	$S_0 \rightarrow S_7$	3.89	319	0.13	HOMO - 5 → LUMO + 1 (11%) HOMO - 4 → LUMO (11%) HOMO - 1 → LUMO + 3 (6%) HOMO → LUMO (37%)
	$S_0 \rightarrow S_8$	3.89	319	0.13	HOMO - 5 → LUMO (11%) HOMO - 4 → LUMO + 1 (11%) HOMO - 1 → LUMO + 4 (6%) HOMO → LUMO + 1 (37%)

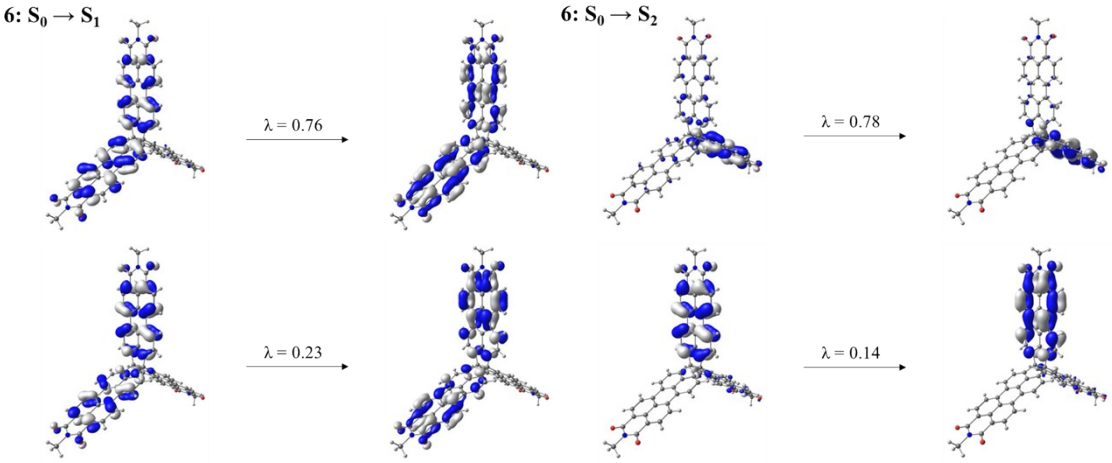

Figure S3. Pictorial representations of hole-electron natural transition orbitals (NTO) of the excitations described in Table S2 for **6** as determined at the TD-OTωB97X-D/6-31g(d,p) level of theory. λ is the fraction of the hole−electron contribution to the excitation.

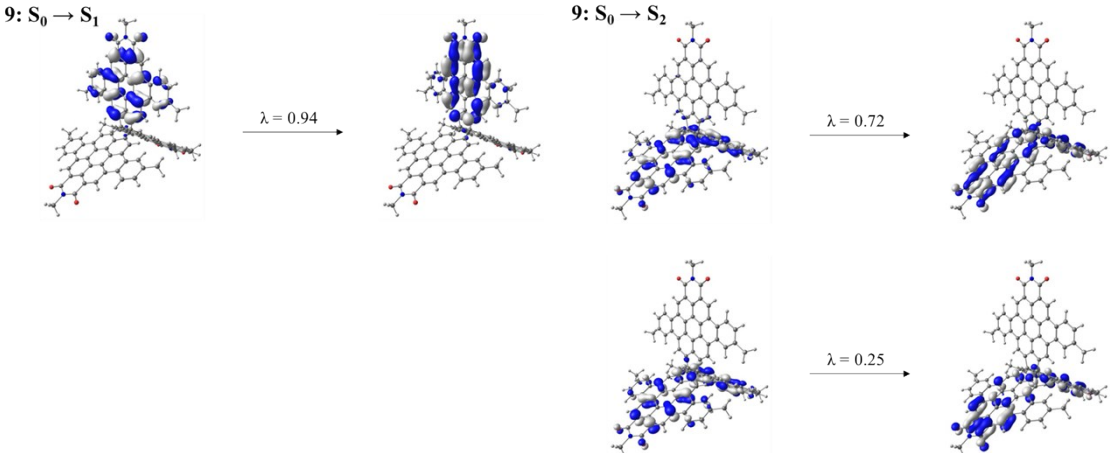

Figure S4. Pictorial representations of hole-electron natural transition orbitals (NTO) of the excitations described in Table S2 for **9** as determined at the TD-OTωB97X-D/6-31g(d,p) level of theory. λ is the fraction of the hole−electron contribution to the excitation.

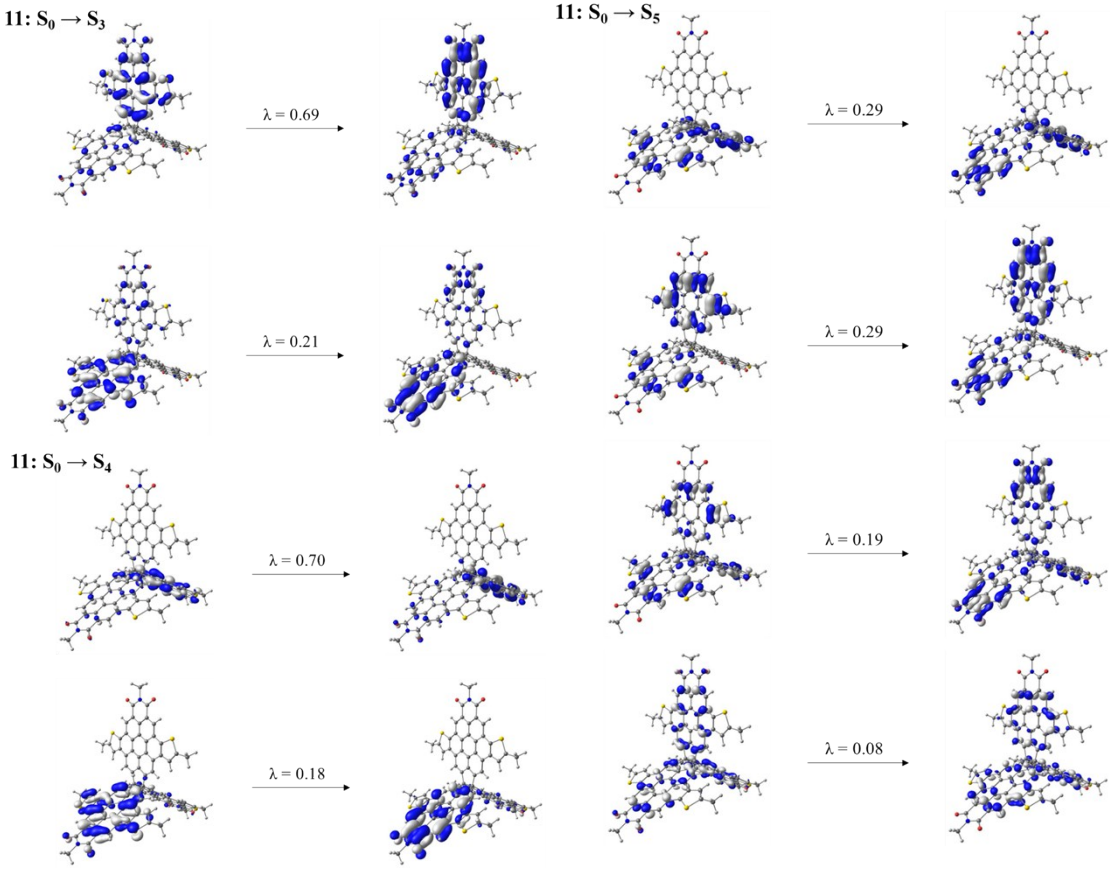

Figure S5. Pictorial representations of hole-electron natural transition orbitals (NTO) of the excitations described in Table S2 for **11** as determined at the TD-OTωB97X-D/6-31g(d,p) level of theory. λ is the fraction of the hole−electron contribution to the excitation.

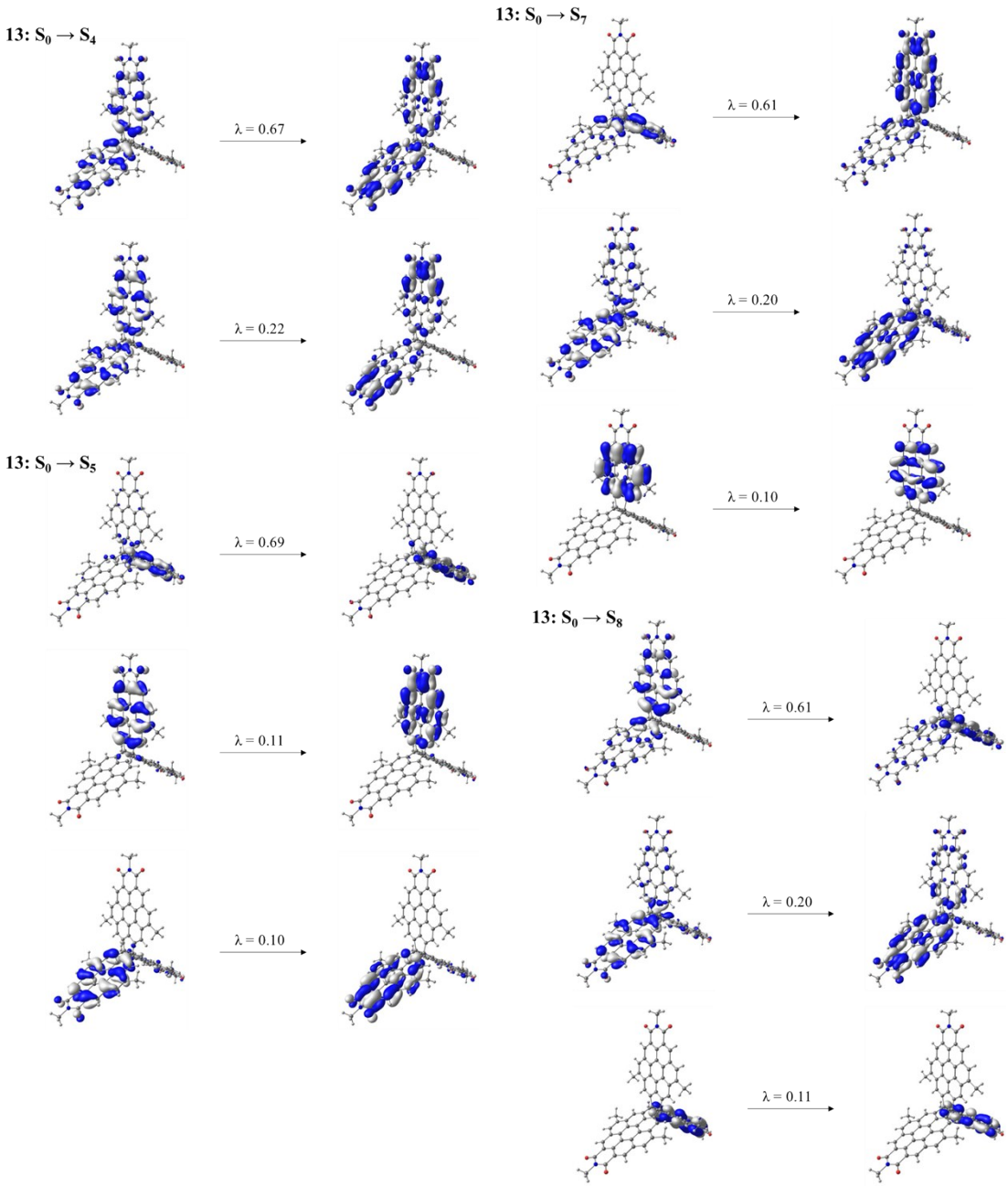

Figure S6. Pictorial representations of hole-electron natural transition orbitals (NTO) of the excitations described in Table S2 for **13** as determined at the TD-OTωB97X-D/6-31g(d,p) level of theory. λ is the fraction of the hole−electron contribution to the excitation.

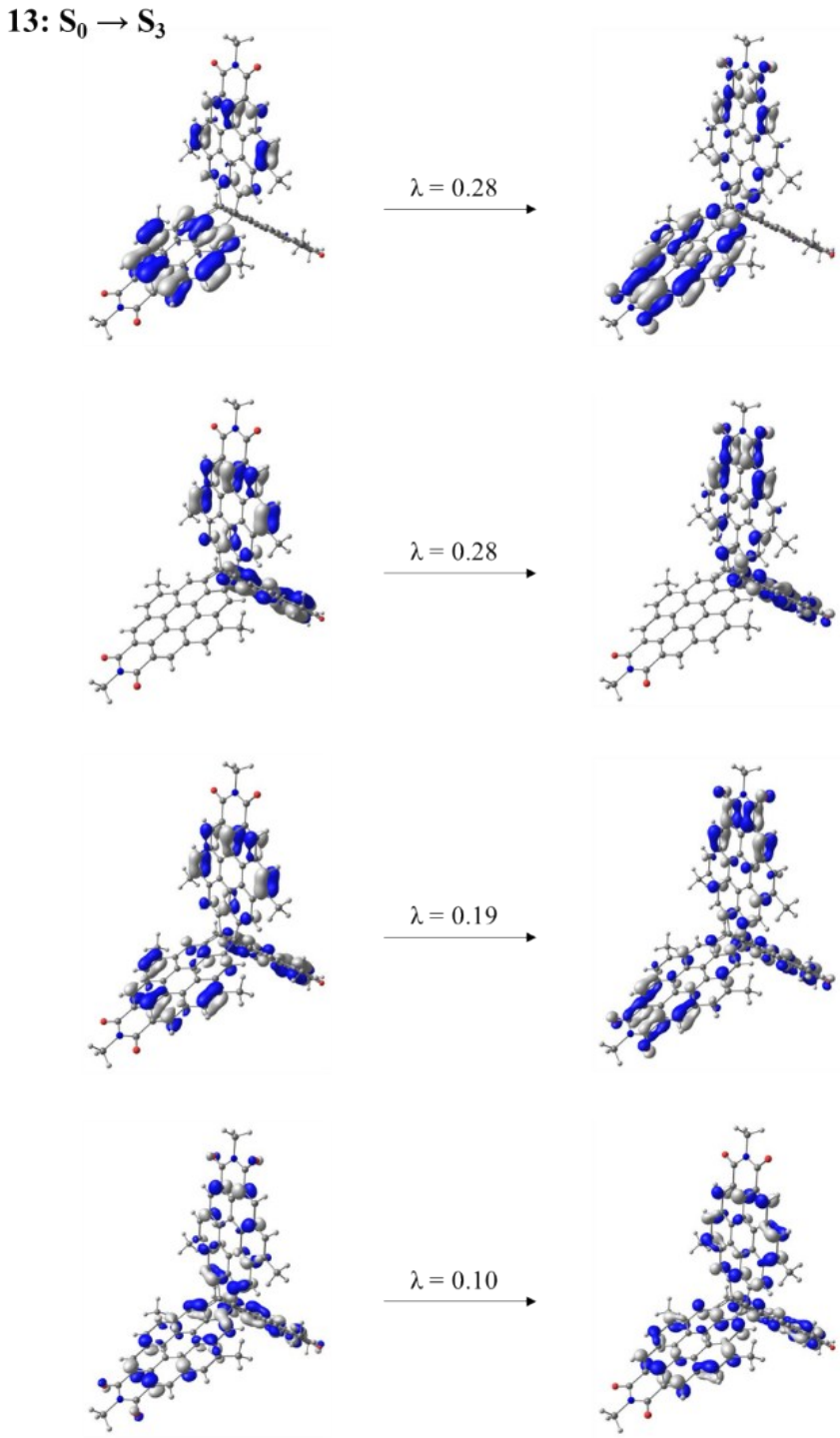

Figure S7. Pictorial representations of hole-electron natural transition orbitals (NTO) of the low-energy transition in **13** that shows PMI-corronene character as determined at the TD-OTωB97X-D/6-31g(d,p) level of theory. λ is the fraction of the hole−electron contribution to the excitation.

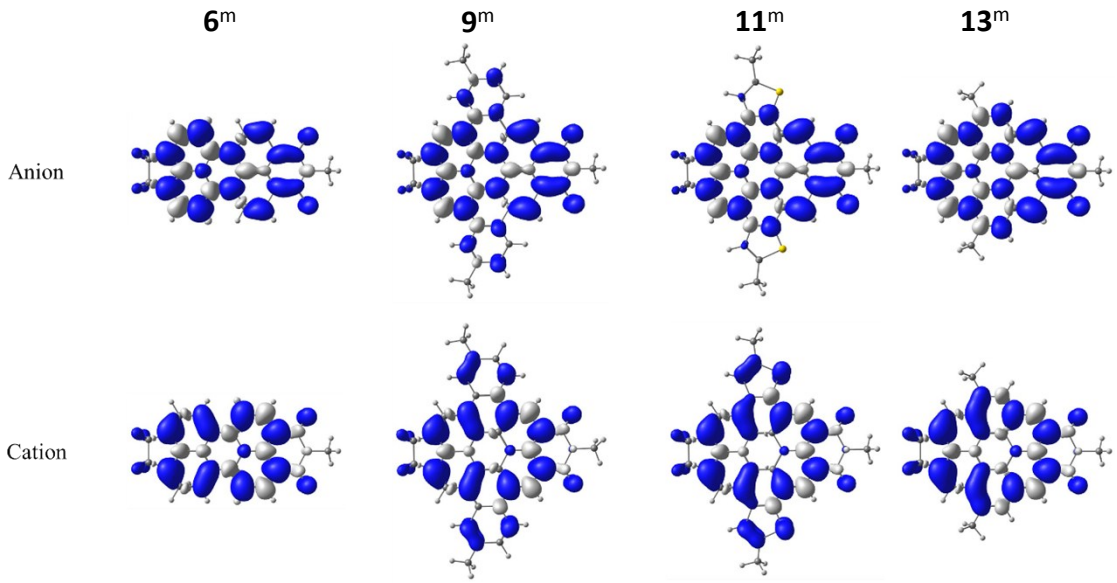

Figure S8. Pictorial representations of the electron spin density in the anion and cation for each of the monomer units as determined at the OT-ωB97X-D/6-31g(d,p) level of theory.

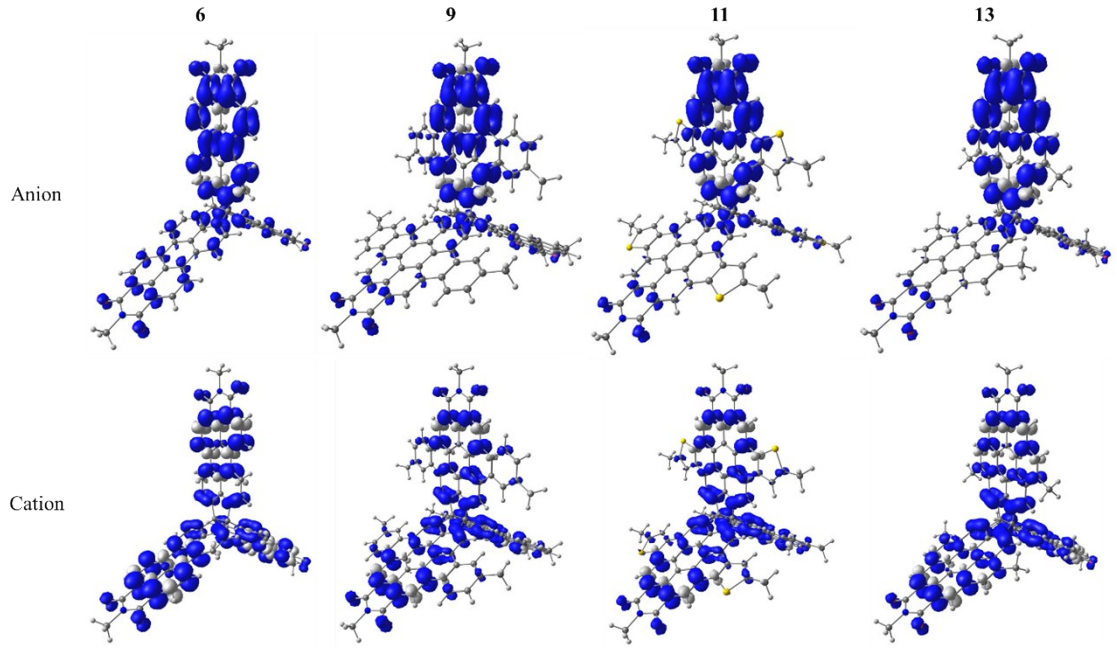

Figure S9. Pictorial representations of the electron spin density in the anion and cation for each of the propellers as determined at the OT-ωB97X-D/6-31g(d,p) level of theory.

Table S4. Photophysical properties, electrochemical data, and DFT calculations for **6**, **9**, **11**, and **13**.

	Uv-Vis [a]				CV [c]				DFT [d]		
	λ_{max} (nm)	ε_{max} (M^{-1} cm^{-1})	λ_{emi} (nm)	Φ_{fl} [b] (%)	$E_{1/2}^{ox}$ (V)	$E_{1/2}^{red}$ (V)	EA (eV)	IP (eV)	EA (eV)	IP (eV)	E_g^{opt} (eV)
6	554	151694	588	85.3	-1.42, -1.88, -2.16, -2.37	0.85, 1.00, 1.20	-3.46	-5.56	-1.99	6.57	2.10
9	492	162737	514	89.3	-1.55, -2.08, -2.13, -2.29	0.99, 1.15, 1.29	-3.29	-5.70	-1.69	6.37	2.38
11	486	136918	505	21.6	-1.56, -1.96, -2.11, -2.25	1.05, 1.22	-3.31	-5.74	-1.62	6.48	2.42
13	432	122061	481	31.6	-1.74, -2.19	1.15, 1.35	-3.13	-5.89	-1.52	6.80	2.52

[a] The photophysical properties of the compounds were measured in $CHCl_3$ (10^{-5} M); [b] Measured in dilute $CHCl_3$ solution (10^{-6} M) and calculated by absolute quantum yield method; [c] CVs were measured in dichloromethane with tetrabutylammonium hexafluorophosphate ($TBAPF_6$, 0.1 M) as the supporting electrolyte with a scan of 100 mv/s; $E_{1/2}^{ox}$ and $E_{1/2}^{red}$ are half-wave potentials of the oxidative and reductive waves (vs Fc/Fc^+); EA and IP values calculated from the onset of the first reduction and oxidation peaks, respectively; [d] The DFT calculations were performed using the OT-ωB97X-D/6-31g(d,p); E_g^{opt} is the optical band gap and estimated from the onset of the absorption peak.

6. OFET fabrication and characterization

Micro/nanometer-sized single-crystals: Micro/nanometer-sized single-crystals of compounds used in this work were prepared in typical growth conditions by drop casting in a sealed bottle with chloroform/toluene as the solvent and isopropyl alcohol as the poor solvent. The single crystals were slowly grown on the OTS modified SiO_2/Si substrates with the solution evaporation.

Devices fabrication: The SiO_2/Si wafers used here were cleaned with deionized water, piranha solution (H_2SO_4/H_2O_2=2:1), deionized water, isopropyl alcohol, and finally were blown dry with high-purity nitrogen gas. Treatment of the SiO_2/Si wafers with octadecyltrichlorosilane (OTS) was conducted by the vapor-deposition method. The clean wafers were dried under vacuum at 90 °C for 2 h to eliminate the moisture. When the temperature is reduced to approximately room temperature, a small drop of OTS was dropped onto the wafers. Subsequently, this system was heated to 120 °C for 2 h under vacuum, after which the vacuum is maintained at approximately room temperature.

Bottom-gate top-contact (BGTC) devices based on the micro/nanometer-sized single crystal were fabricated respectively with the organic ribbon mask method.[11] Firstly, an individual organic nanowire was put directly on a crystal perpendicularly to the growth direction; secondly, a layer of Au about 80 nm thick was deposited as the source and drain electrodes; finally, the organic nanowires were removed and a transistor with two electrodes was obtained. All electrical characteristics of the devices were measured at room temperature using a semiconductor parameter analyser (Keithley 4200 SCS) and Micromanipulator 6150 probe station. The mobility of the devices were calculated in the saturation

regime. The equation is listed as follows:

$$I_{DS}=(W/2L)C_i\mu(V_{GS}-V_T)^2$$

where W/L is the channel width/length , C_i is the insulator capacitance per unit area, and V_{GS} and V_T are the gate voltage and threshold voltage, respectively.

Devices characterization: The microscope images of all the aligned microcrystal arrays were acquired by an optical microscope (Vision Engineering Co., UK), which was coupled to a CCD camera. Atomic force microscopy (AFM) measurements were carried out with a Nanoscope IIIa instrument (Digital Instruments). SEM images were obtained with a Hitachi S-4300 microscope (Japan). X-ray diffraction (XRD) was measured on a D/max2500 with a CuKα source (κ = 1.541 Å). TEM observation was carried out with a JEOL 1011 JEM-2100F microscope operated at 200 kV.

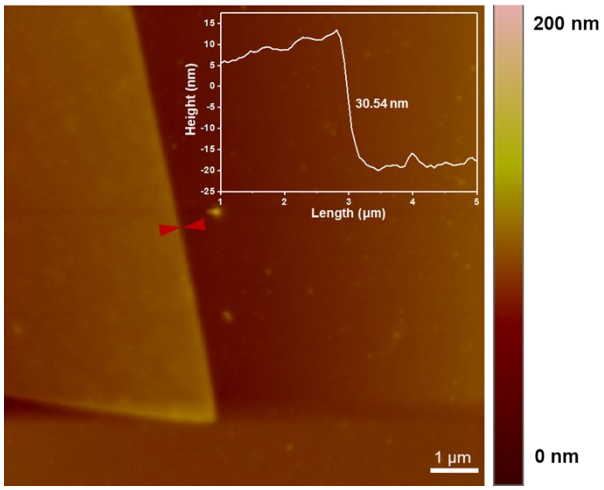

Figure S10. Atomic force microscopy (AFM) of **9** microcrystal.

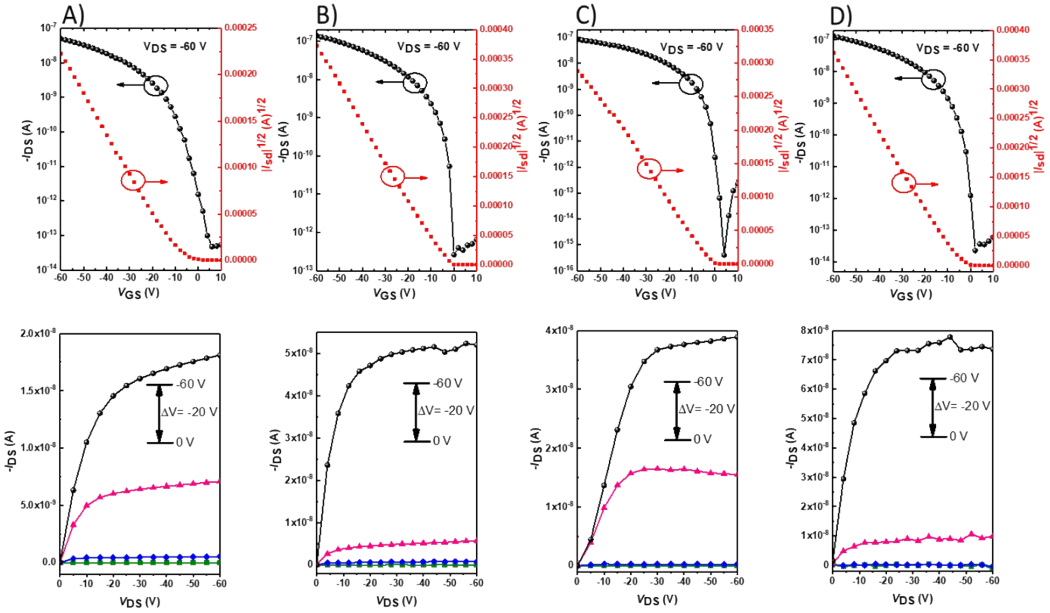

Figure S11. Transfer (top) and output (bottom) characteristics of the different conducting channels of the OFET devices based on **9** microcrystals: A) 1↔2, B) 2↔3, C) 3↔4, and D) 4↔1.

Table S5. Single-crystal transistor characteristics of **9**.

Device channel	W/L (μm)	μ_{max} ($cm^2V^{-1}s^{-1}$)	V_t (V)	On/off Ratio
1↔2	4.7/6.4	4.92×10^{-3}	-8.1	1.0×10^{6}
2↔3	7.1/3.8	4.55×10^{-3}	-3.1	5.3×10^{5}
3↔4	6.7/6.4	4.95×10^{-3}	-1.3	6.2×10^{6}
4↔1	7.3/3.8	4.51×10^{-3}	-5.2	5.7×10^{6}

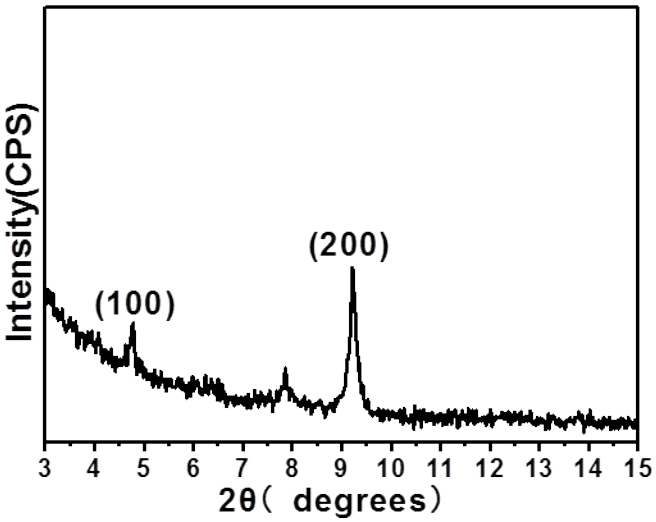

Figure S12. XRD of **9** microcrystals.

7. References

[1] Kubo, T.; Miyazaki, S.; Kodama, T.; Aoba, M.; Hirao, Y.; Kuratab, H. *Chem. Commun*. **2015**, *51*, 3801-3803.

[2] Chai, J.-D.; Head-Gordon, M. *Phys. Chem. Chem. Phys*. **2008**, *10*, 6615-6620.

[3] Francl, M. M.; Pietro, W. J.; Hehre, W. J.; Binkley, J. S.; Gordon, M. S.; DeFrees, D. J.; Pople, J. A. *J. Chem. Phys*. **1982**, *77*, 3654-3665.

[4] Hariharan, P. C.; Pople, J. A. *Theor. Chem. Acc*. **1973**, *28*, 213-222.

[5] Stein, T.; Kronik, L.; Baer, R. *J. Am. Chem. Soc*. **2009**, *131*, 2818-2820.

[6] Stein, T.; Eisenberg, H.; Kronik, L.; Baer, R. *Phys. Rev. Lett*. **2010**, *105*, 266802.

[7] Stein, T.; Kronik, L.; Baer, R. *J. Chem. Phys*. **2009**, *131*, 244119.

[8] Refaely-Abramson, S.; Baer, R.; Kronik, L. *Phys. Rev. B* **2011**, *84*, 075144.

[9] Sutton, C.; Körzdörfer, T.; Coropceanu, V.; Brédas, J.-L. *J. Phys. Chem. C* **2014**, *118*, 3925-3934.

[10] Körzdörfer, T.; Sears, J. S.; Sutton, C.; and Brédas, J.-L. *J. Chem. Phys*. **2001**, *135*, 204107.

[11] Li, R.; Jiang, L.; Meng, Q.; Gao, J.; Li, H.; Tang, Q.; He, M.; Hu, W.; Liu, Y.; Zhu, D. *Adv. Mater*. **2009**, *21*, 4492-4495.

8. ^{1}H NMR, and ^{13}C NMR Spectra of Compounds

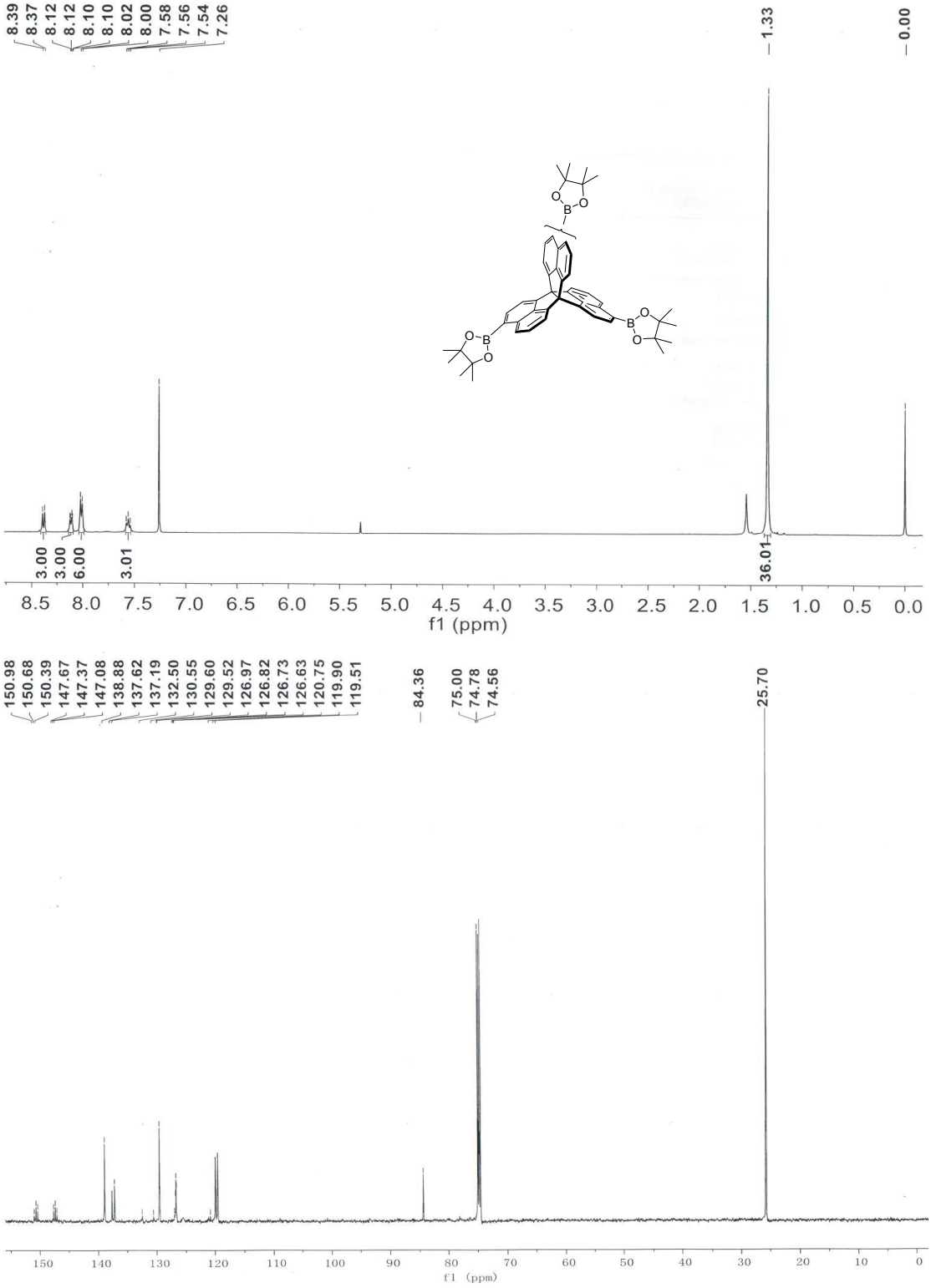

Figure S13. ^{1}H NMR and ^{13}C NMR (bottom) of **3**. (^{1}H NMR in $CDCl_3$ at 27 ^{o}C; ^{13}C NMR in $C_2D_2Cl_4$ at 100 ^{o}C)

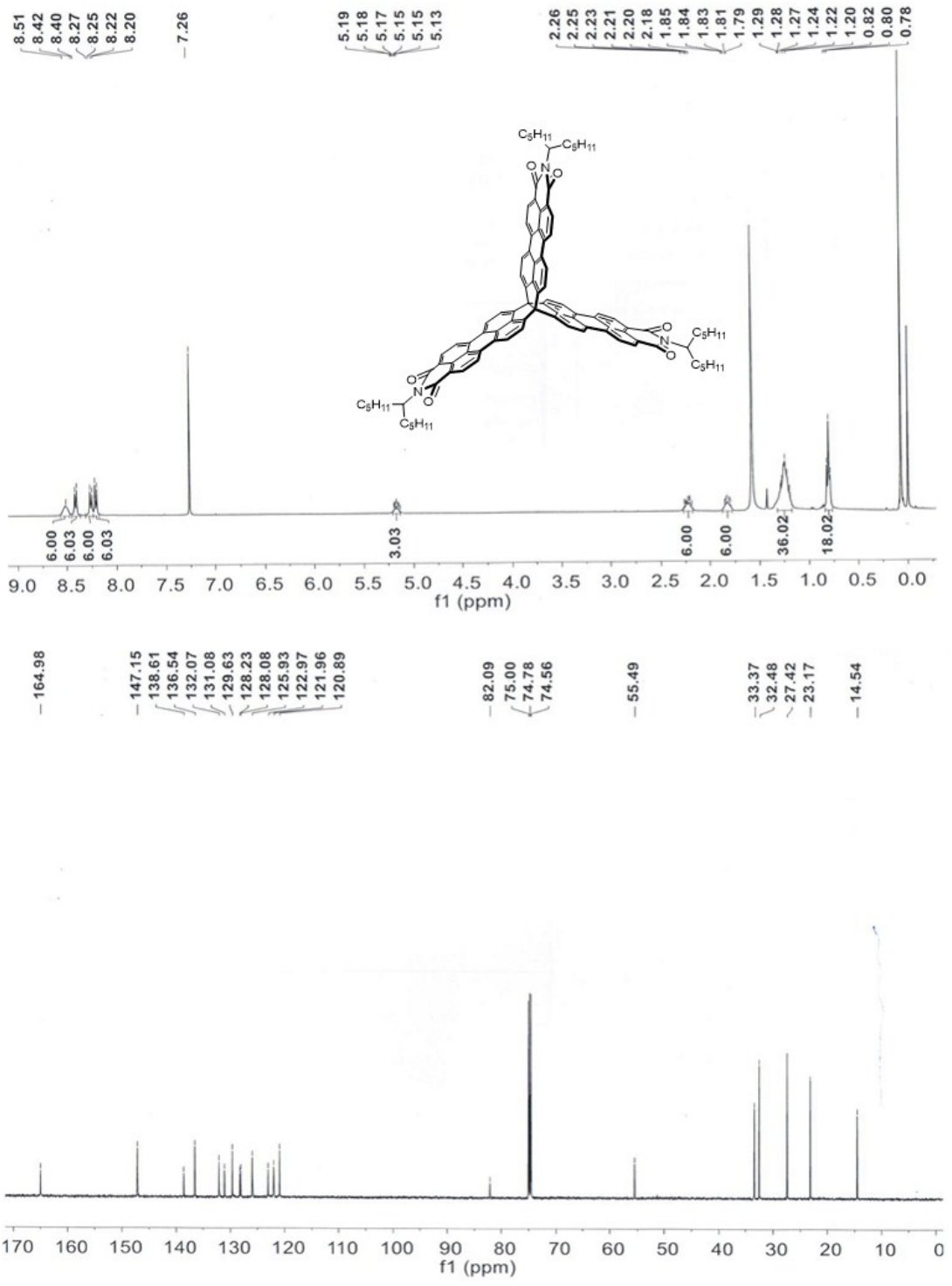

Figure S14. ^{1}H NMR and ^{13}C NMR (bottom) of **6**. (^{1}H NMR in $CDCl_3$ at 27 ^{o}C; ^{13}C NMR in $C_2D_2Cl_4$ at 100 ^{o}C)

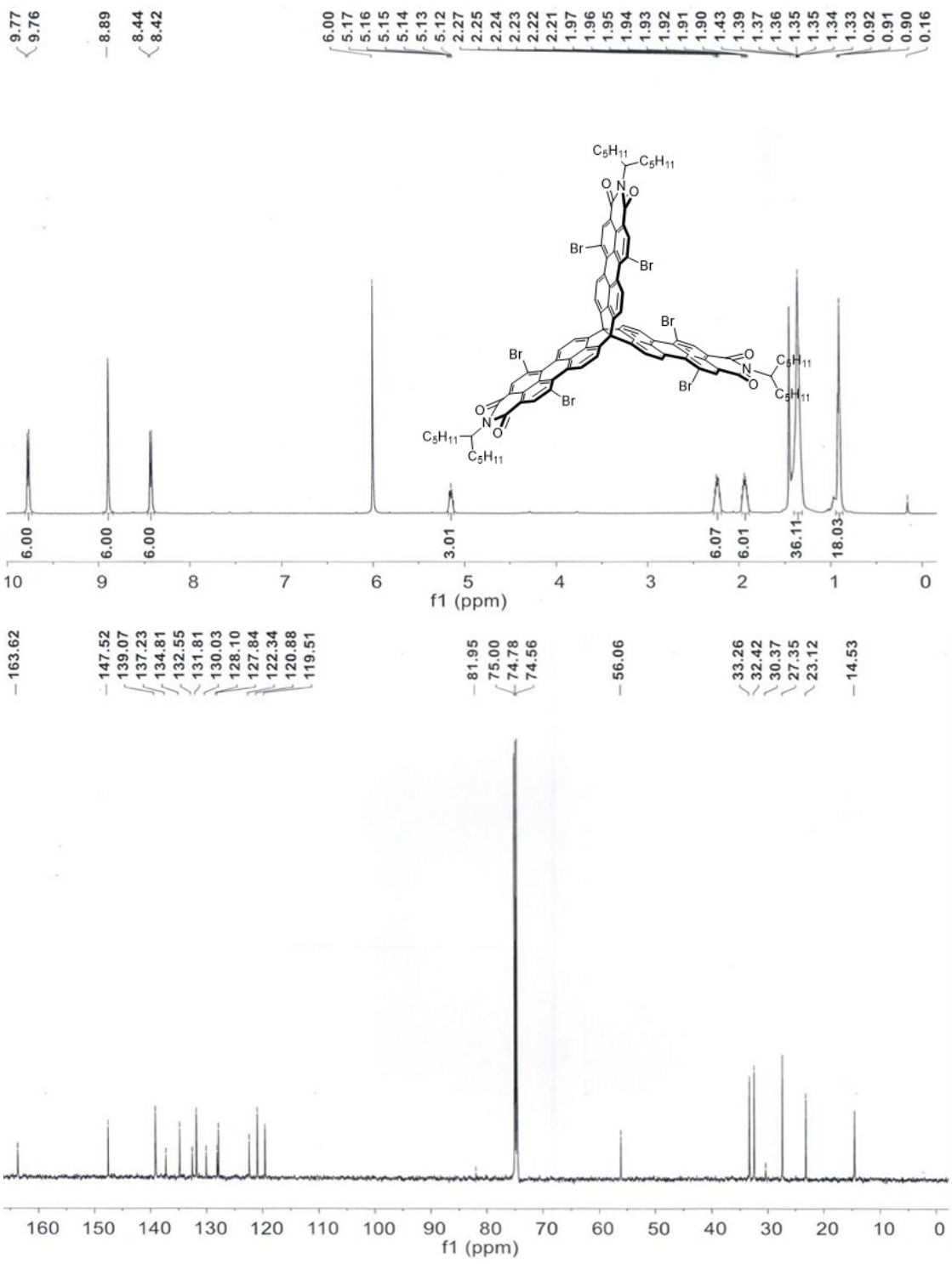

Figure S15. ^{1}H NMR and ^{13}C NMR (bottom) of **7**. (^{1}H NMR in $C_2D_2Cl_4$ at 100 ^{o}C; ^{13}C NMR in $C_2D_2Cl_4$ at 100 ^{o}C)

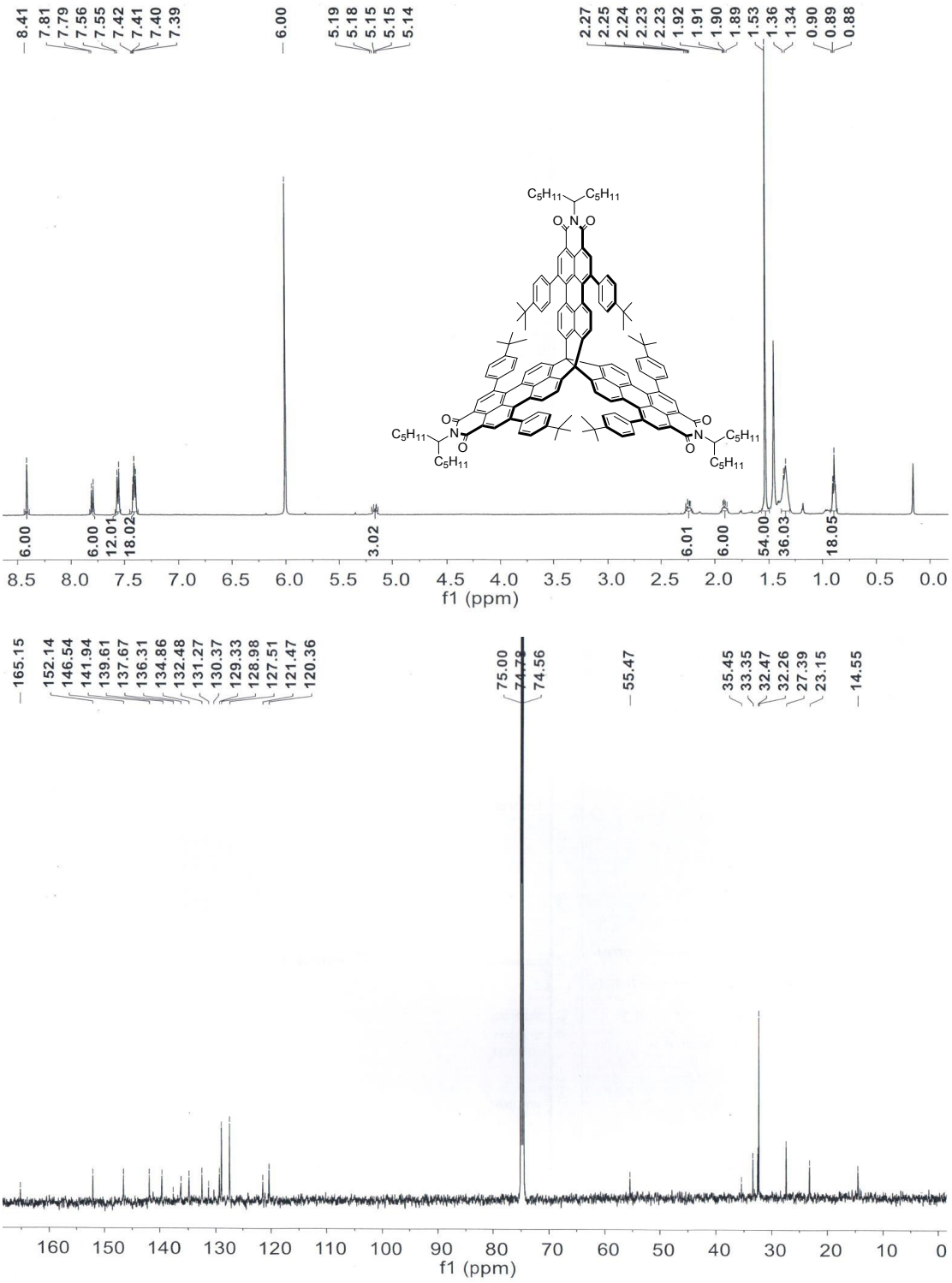

Figure S16. ^{1}H NMR and ^{13}C NMR (bottom) of **8**. (^{1}H NMR in $C_2D_2Cl_4$ at 100 ^{o}C; ^{13}C NMR in $C_2D_2Cl_4$ at 100 ^{o}C.

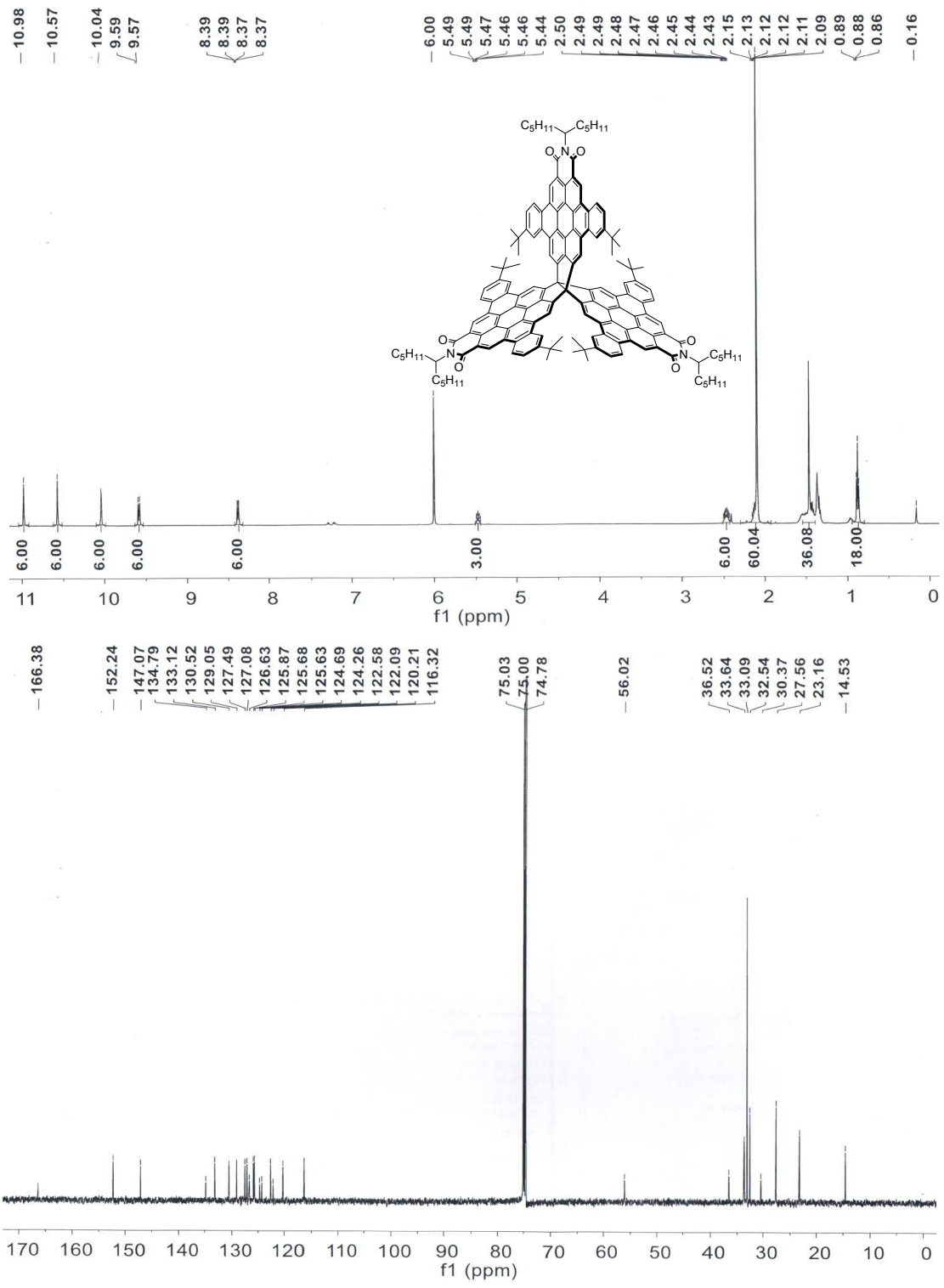

Figure S17. ^{1}H NMR and ^{13}C NMR (bottom) of **9**. (^{1}H NMR in $C_2D_2Cl_4$ at 100 ^{o}C; ^{13}C NMR in $C_2D_2Cl_4$ at 100 ^{o}C)

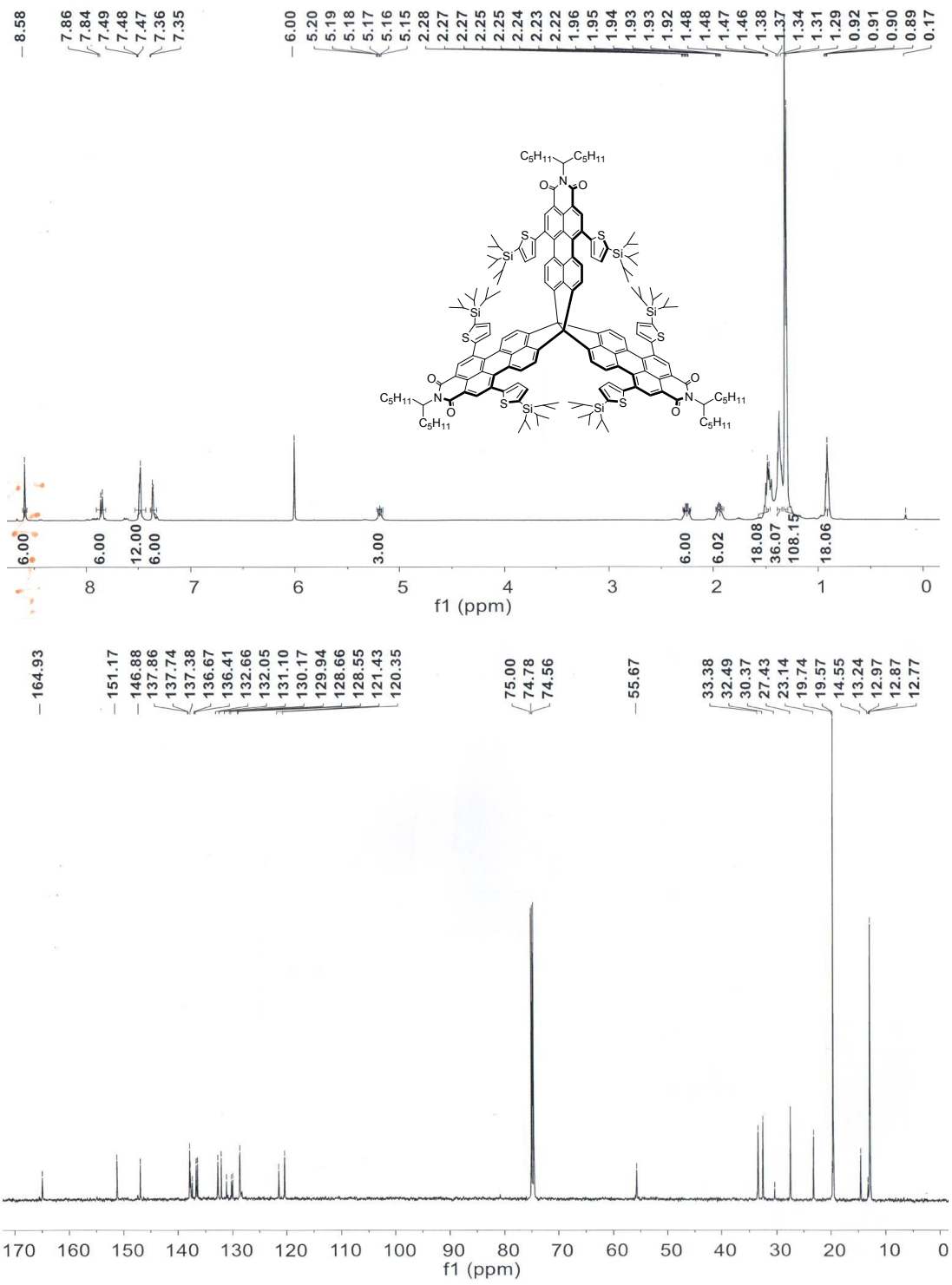

Figure S18. ^{1}H NMR and ^{13}C NMR (bottom) of **10**. (^{1}H NMR in $C_2D_2Cl_4$ at 100 ^{o}C; ^{13}C NMR in $C_2D_2Cl_4$ at 100 ^{o}C)

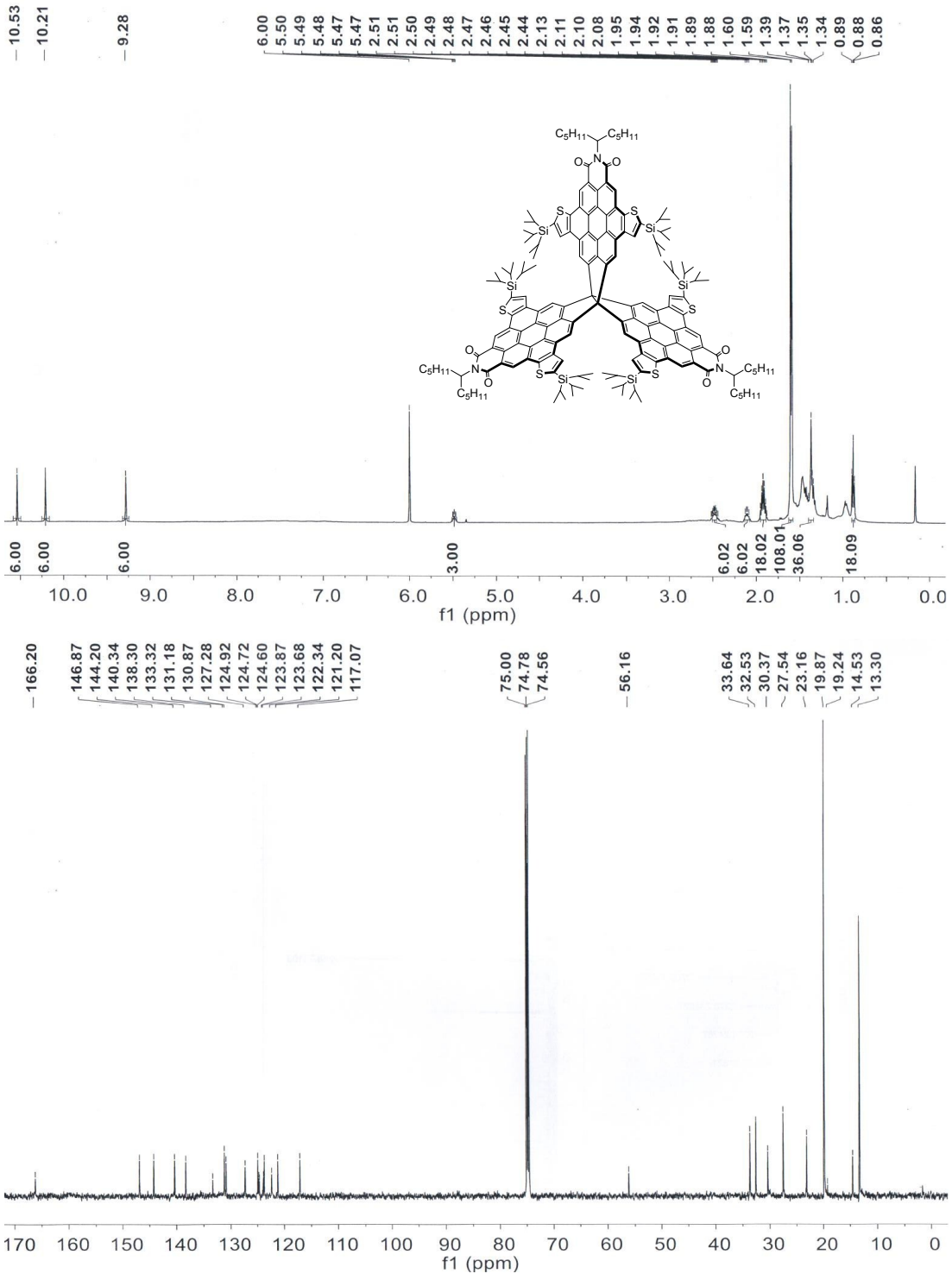

Figure S19. ^{1}H NMR and ^{13}C NMR (bottom) of **11**. (^{1}H NMR in $C_2D_2Cl_4$ at 100 ^{o}C; ^{13}C NMR in $C_2D_2Cl_4$ at 100 ^{o}C)

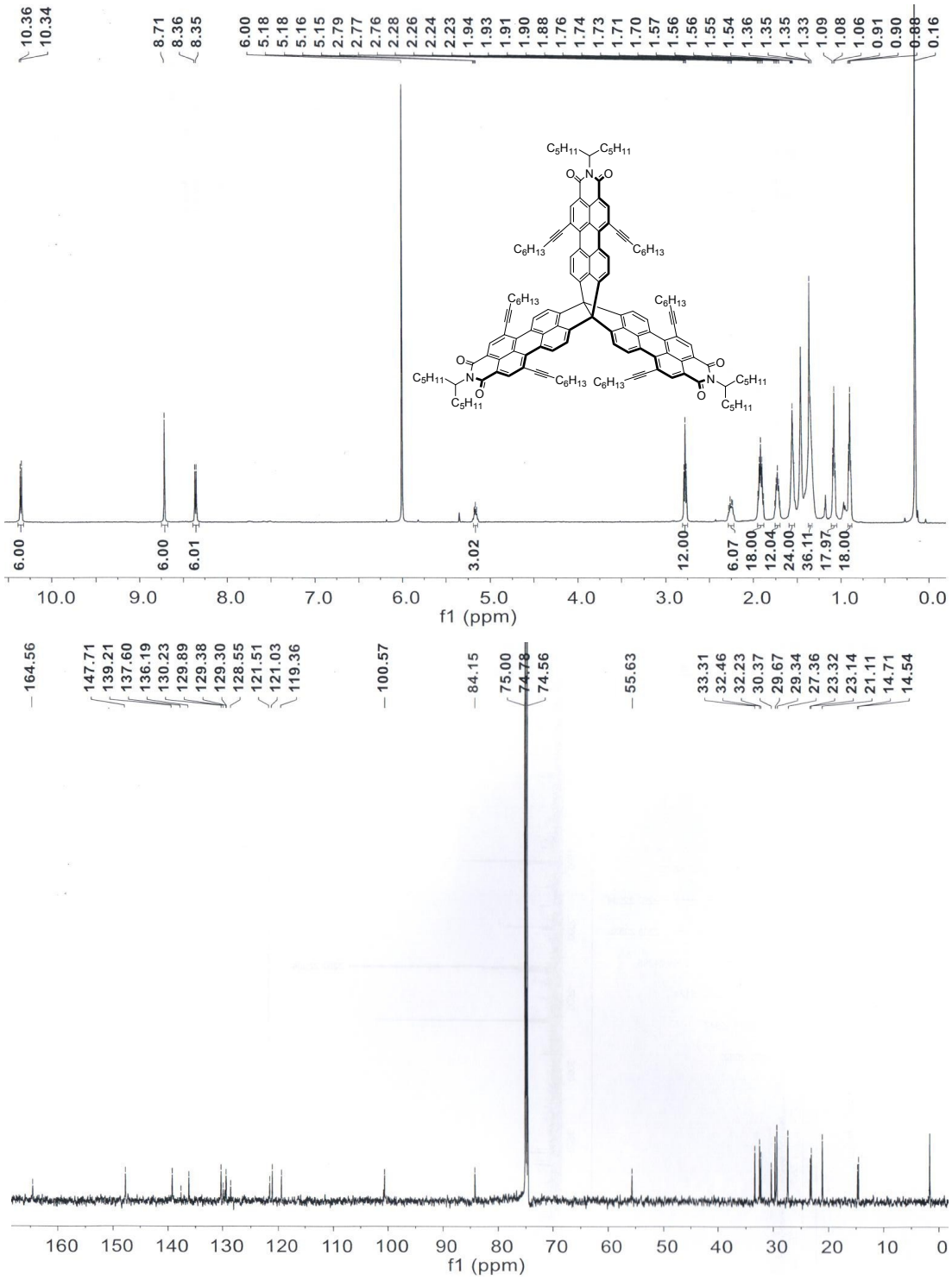

Figure S20. ^{1}H NMR and ^{13}C NMR (bottom) of **12**. (^{1}H NMR in $C_2D_2Cl_4$ at 100 ^{o}C; ^{13}C NMR in $C_2D_2Cl_4$ at 100 ^{o}C)

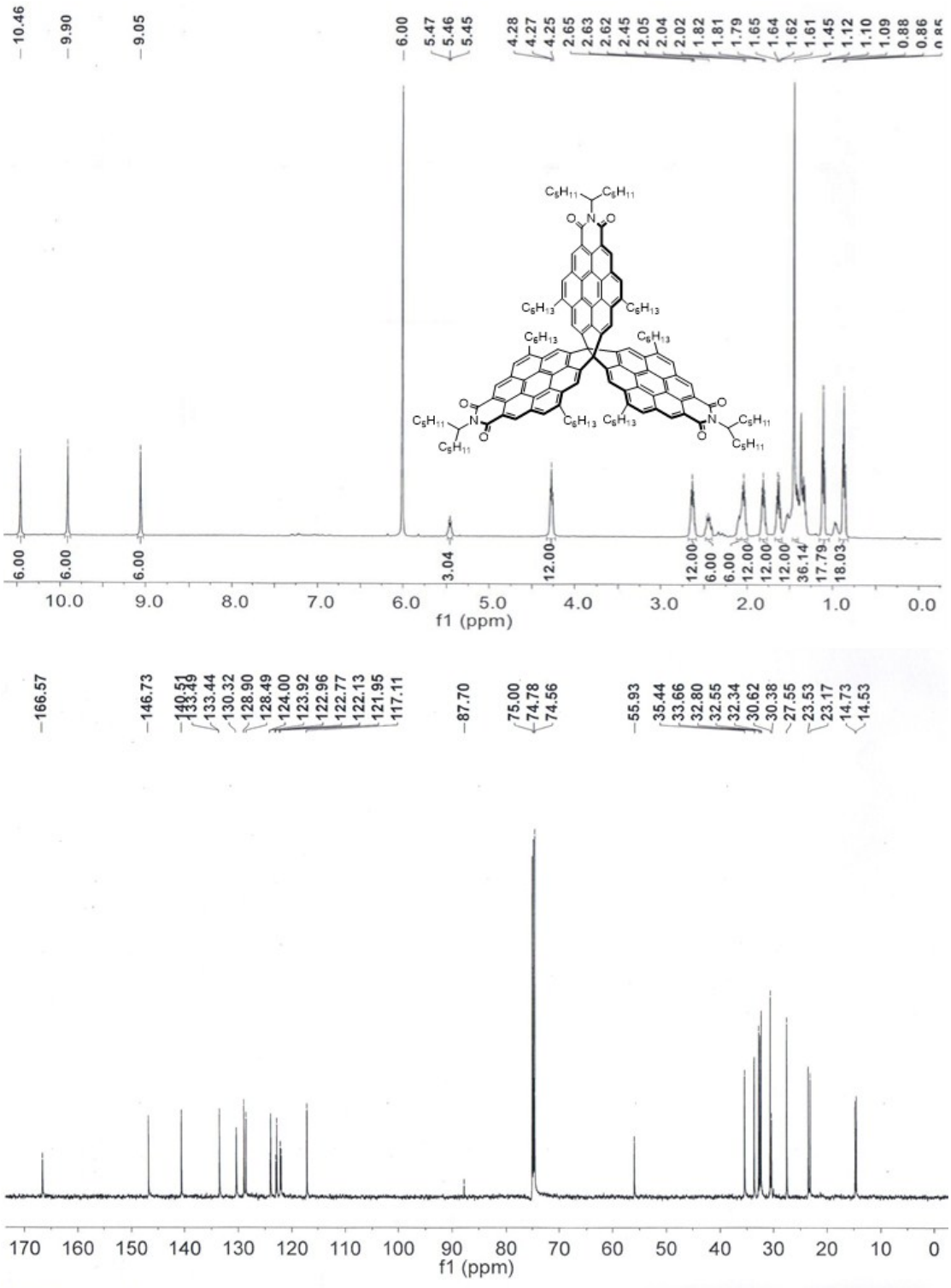

Figure S21. ^{1}H NMR and ^{13}C NMR (bottom) of **13**. (^{1}H NMR in $C_2D_2Cl_4$ at 100 °C; ^{13}C NMR in $C_2D_2Cl_4$ at 100 °C)

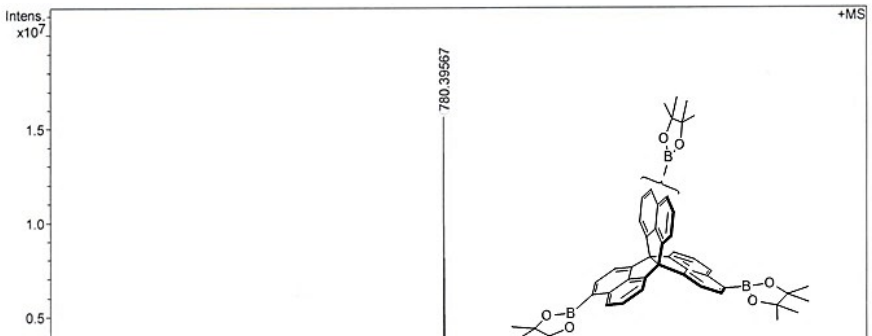

Figure S22. HRMS spectra of **3**.

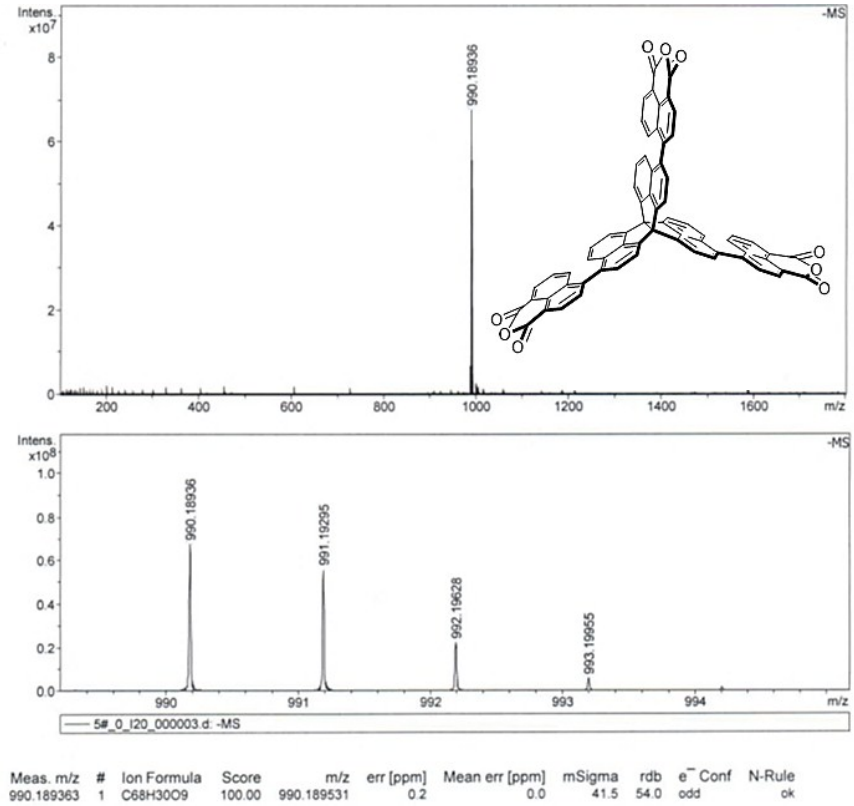

Meas. m/z	#	Ion Formula	Score	m/z	err [ppm]	Mean err [ppm]	mSigma	rdb	e⁻ Conf	N-Rule
990.189363	1	C68H30O9	100.00	990.189531	0.2	0.0	41.5	54.0	odd	ok

Figure S23. HRMS spectra of **4**.

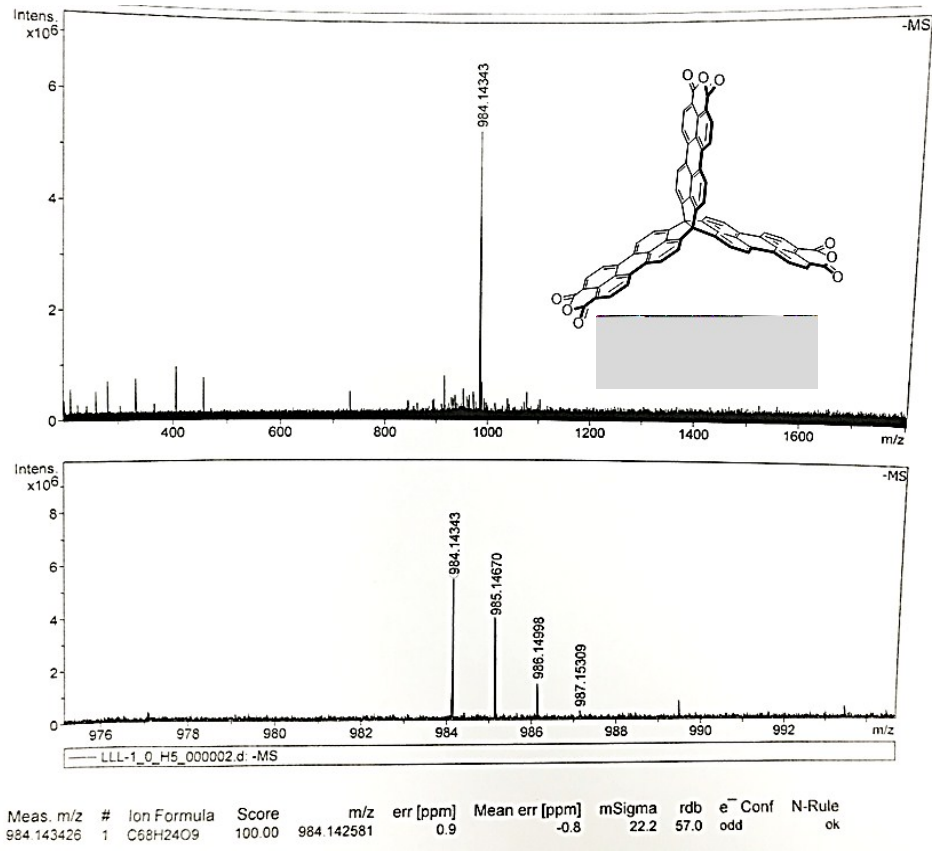

Meas. m/z	#	Ion Formula	Score	m/z	err [ppm]	Mean err [ppm]	mSigma	rdb	e⁻ Conf	N-Rule
984.143426	1	C68H24O9	100.00	984.142581	0.9	-0.8	22.2	57.0	odd	ok

Figure S24. HRMS spectra of **5**.

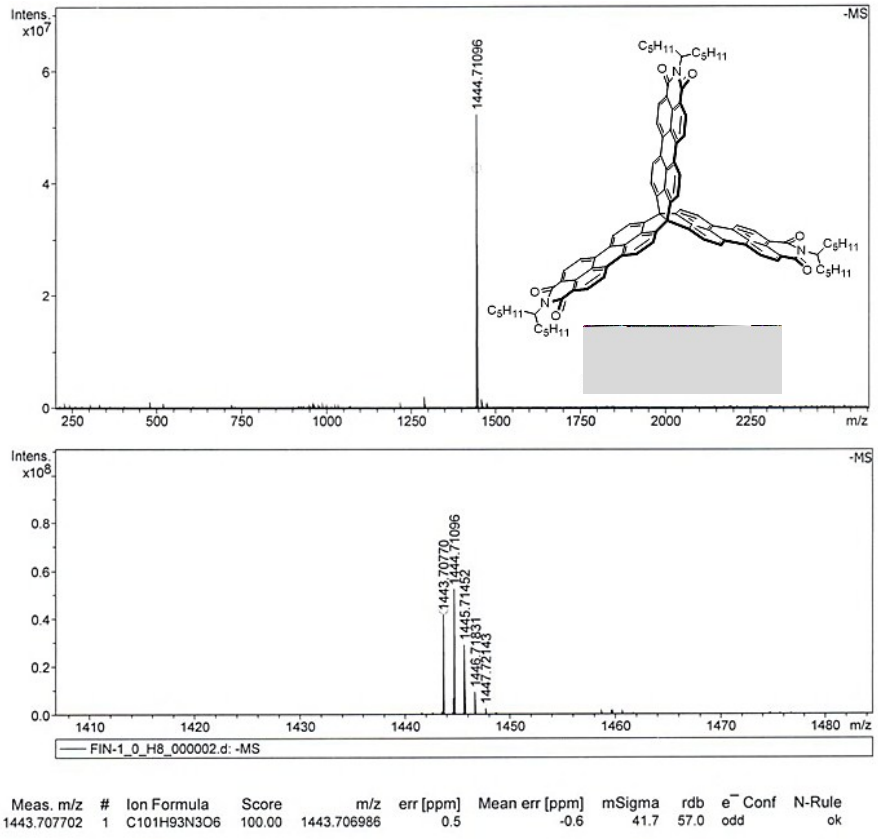

Meas. m/z	#	Ion Formula	Score	m/z	err [ppm]	Mean err [ppm]	mSigma	rdb	e⁻ Conf	N-Rule
1443.707702	1	C101H93N3O6	100.00	1443.706986	0.5	-0.6	41.7	57.0	odd	ok

Figure S25. HRMS spectra of **6**.

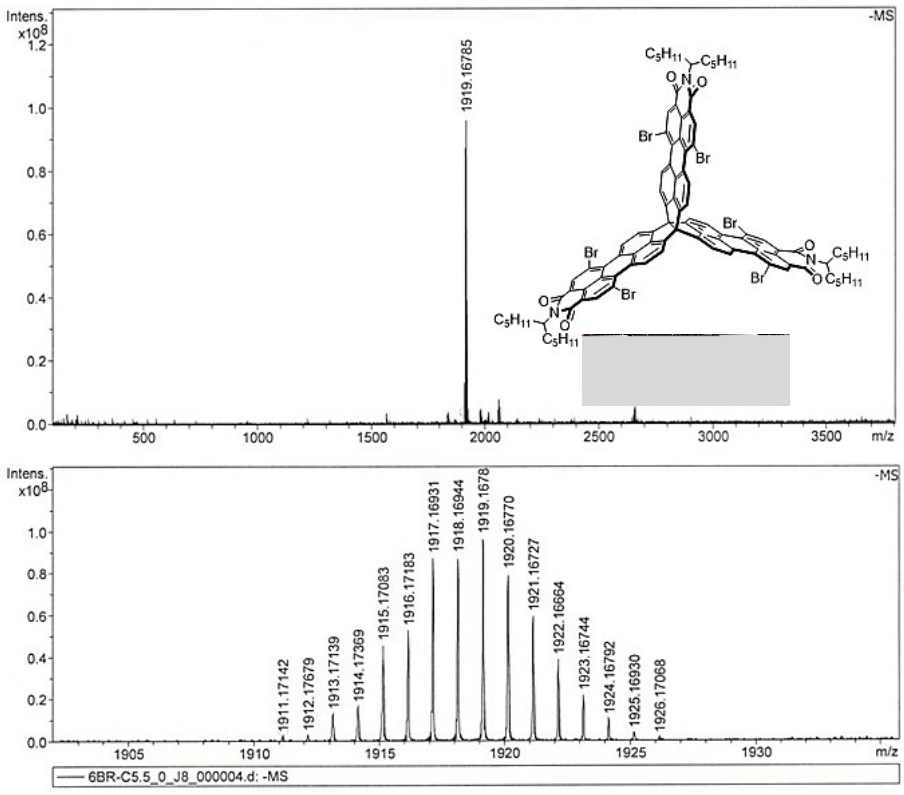

Meas. m/z	#	Ion Formula	Score	m/z	err [ppm]	Mean err [ppm]	mSigma	rdb	e⁻ Conf	N-Rule
1911.171421	1	C101H87Br6N3O6	100.00	1911.170059	-0.7	-0.7	75.7	57.0	odd	ok

Figure S26. HRMS spectra of **7**.

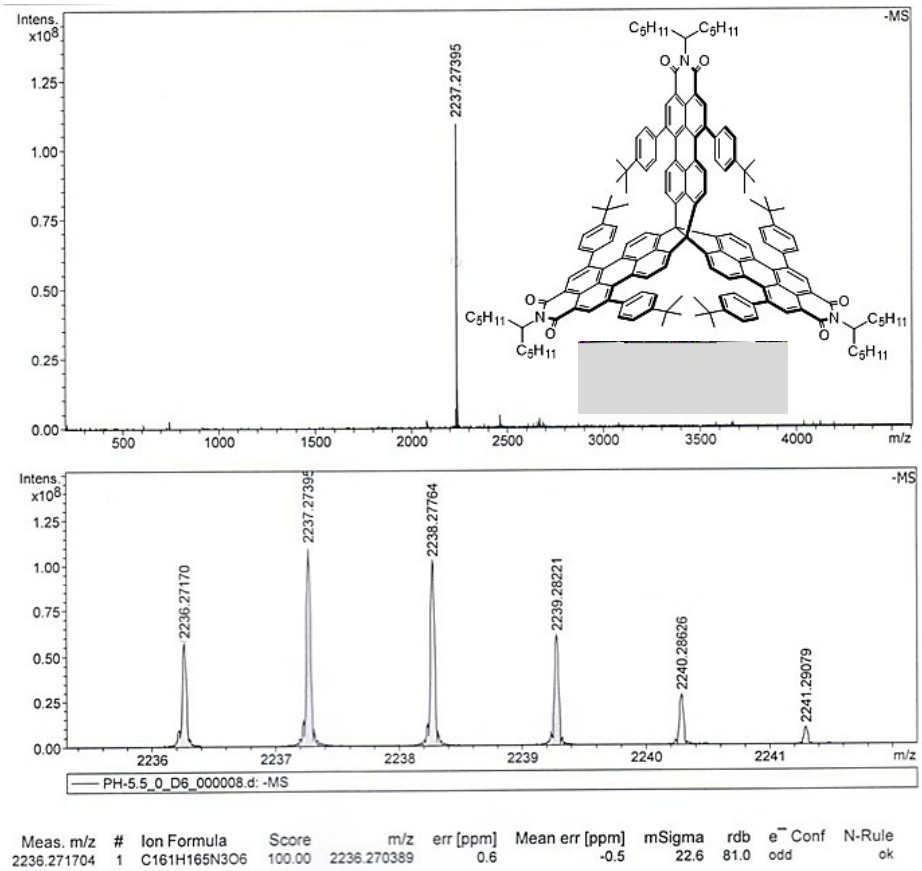

Meas. m/z	#	Ion Formula	Score	m/z	err [ppm]	Mean err [ppm]	mSigma	rdb	e⁻ Conf	N-Rule
2236.271704	1	C161H165N3O6	100.00	2236.270389	0.6	-0.5	22.6	81.0	odd	ok

Figure S27. HRMS spectra of **8**.

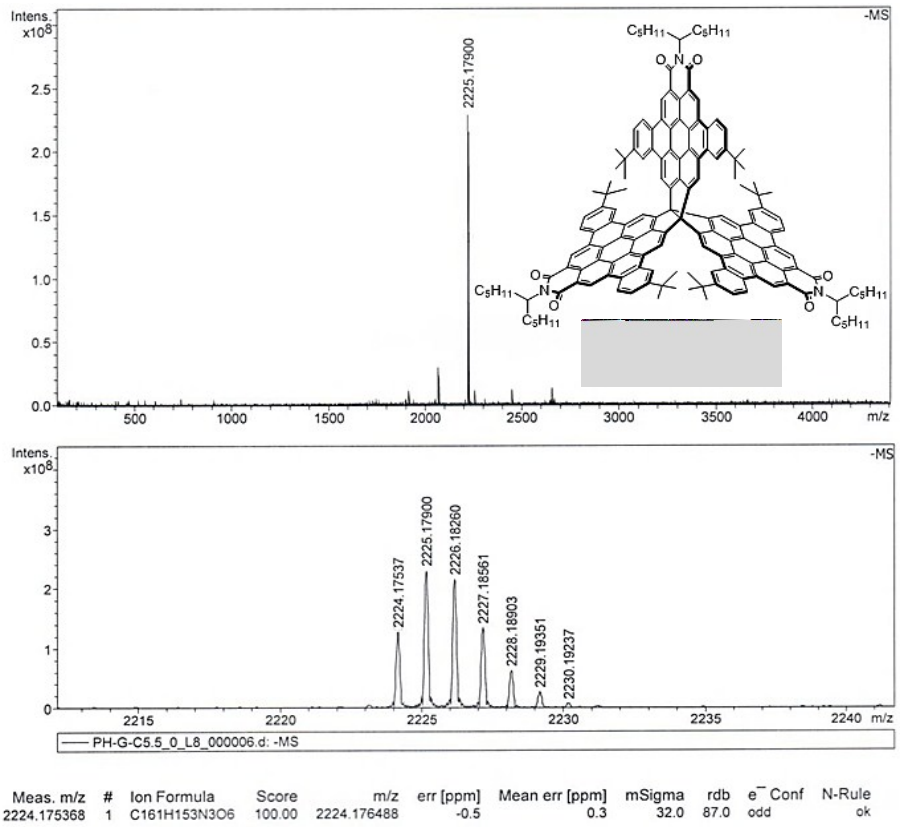

Meas. m/z	#	Ion Formula	Score	m/z	err [ppm]	Mean err [ppm]	mSigma	rdb	e⁻ Conf	N-Rule
2224.175368	1	C161H153N3O6	100.00	2224.176488	-0.5	0.3	32.0	87.0	odd	ok

Figure S28. HRMS spectra of **9**.

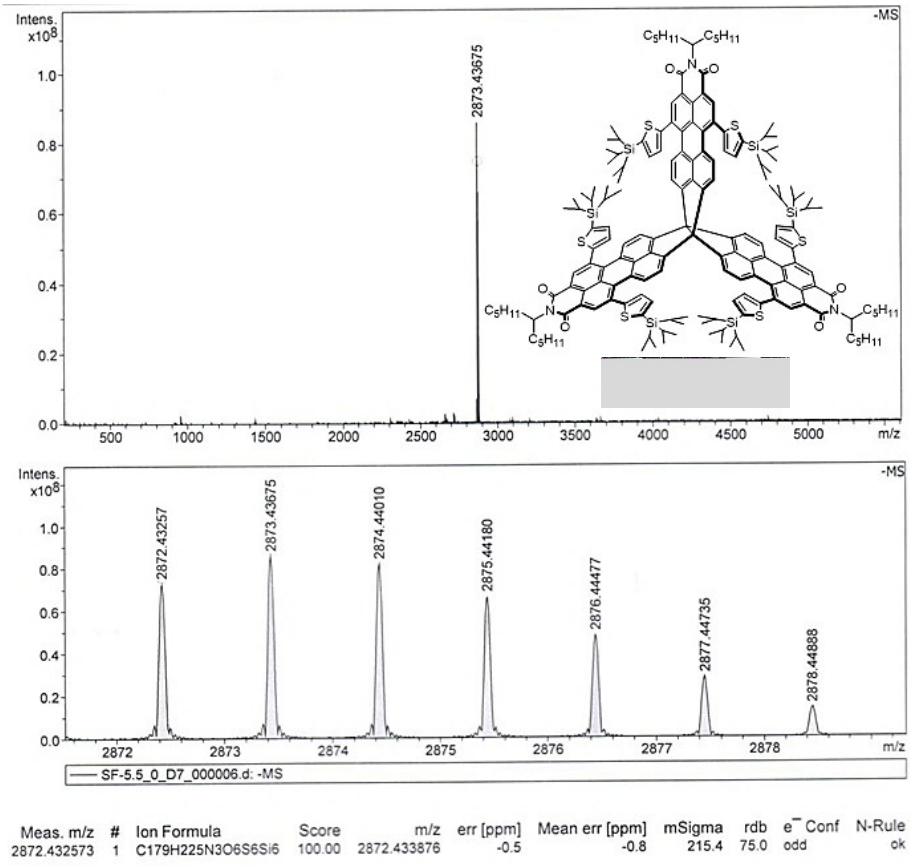

Meas. m/z	#	Ion Formula	Score	m/z	err [ppm]	Mean err [ppm]	mSigma	rdb	e⁻ Conf	N-Rule
2872.432573	1	C179H225N3O6S6Si6	100.00	2872.433876	-0.5	-0.8	215.4	75.0	odd	ok

Figure S29. HRMS spectra of **10**.

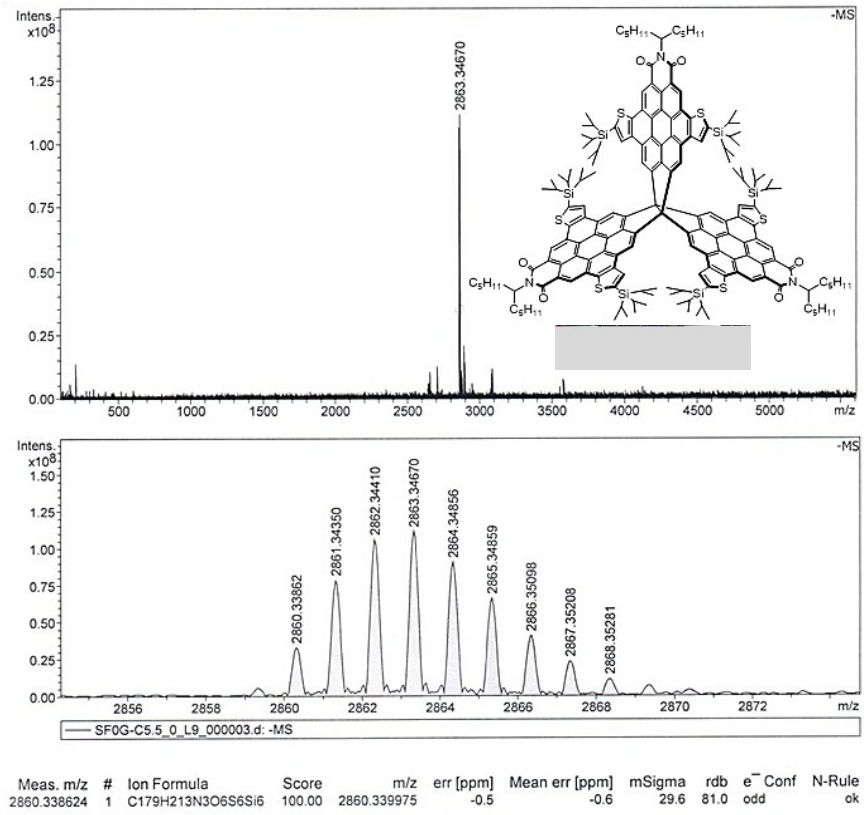

Meas. m/z	#	Ion Formula	Score	m/z	err [ppm]	Mean err [ppm]	mSigma	rdb	e⁻ Conf	N-Rule
2860.338624	1	C179H213N3O6S6Si6	100.00	2860.339975	-0.5	-0.6	29.6	81.0	odd	ok

Figure S30. HRMS spectra of **11**.

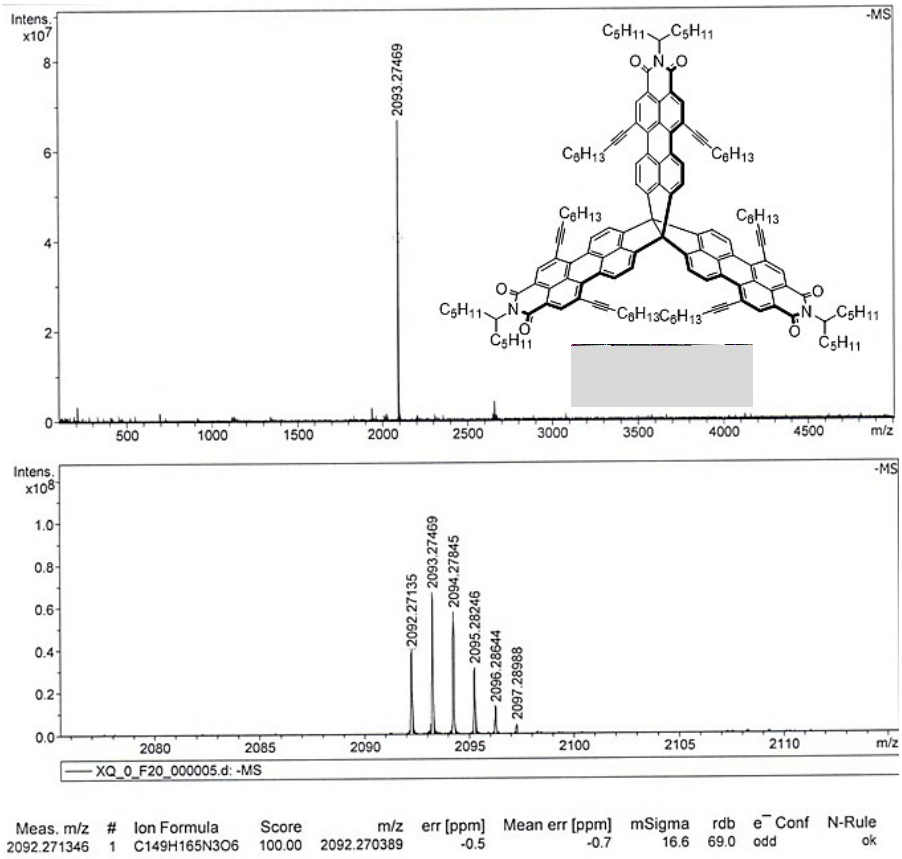

Meas. m/z	#	Ion Formula	Score	m/z	err [ppm]	Mean err [ppm]	mSigma	rdb	e⁻ Conf	N-Rule
2092.271346	1	C149H165N3O6	100.00	2092.270389	-0.5	-0.7	16.6	69.0	odd	ok

Figure S31. HRMS spectra of **12**.

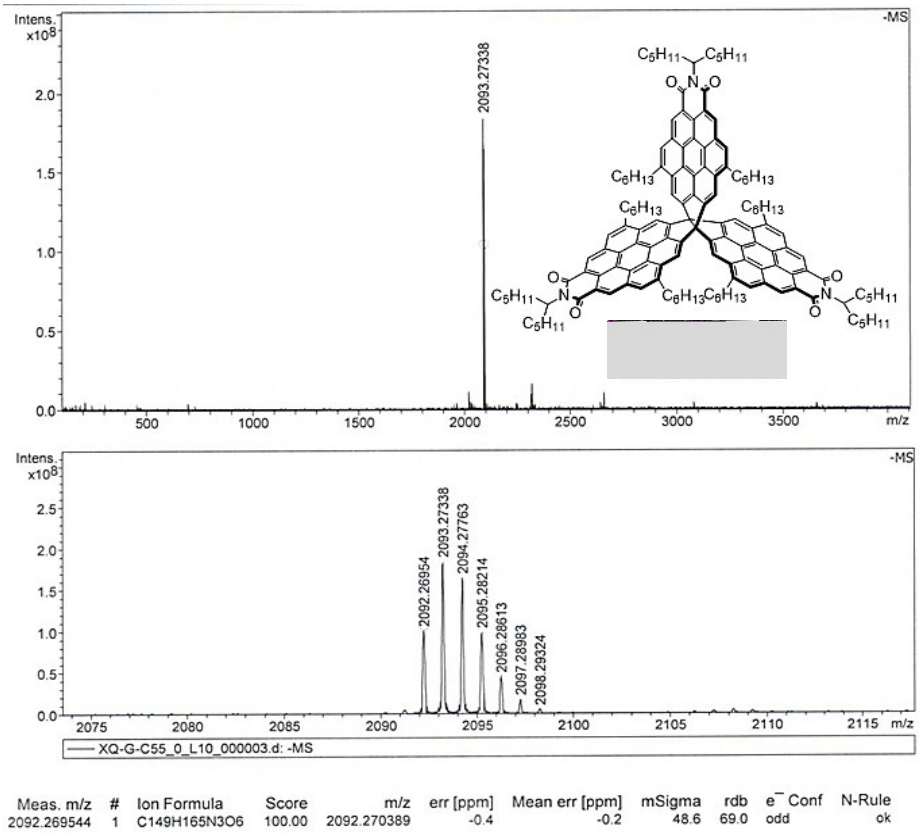

Figure S32. HRMS spectra of **13**.

9. HMBC and 1D NOE Spectra of Compounds

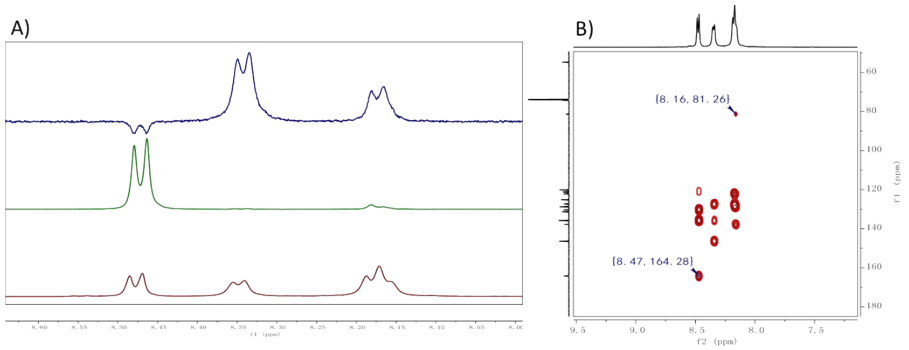

Figure S33. Aromatic region of 1D NOE (A) and HMBC (B) of **6**.

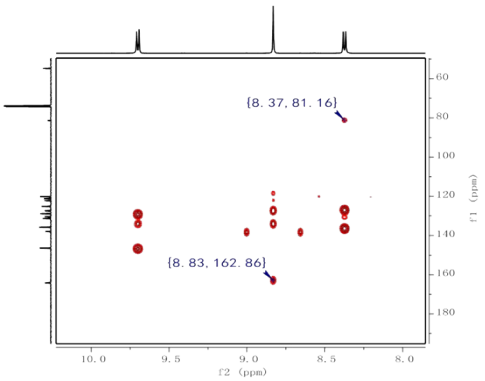

Figure S34. Aromatic region of HMBC of **7**.

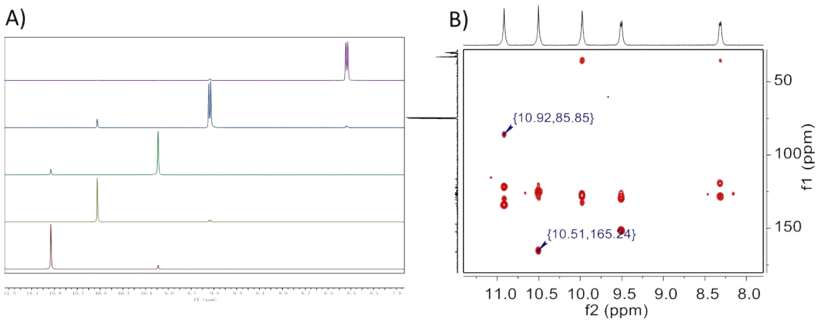

Figure S35. Aromatic region of 1D NOE (A) and HMBC (B) of **9**.

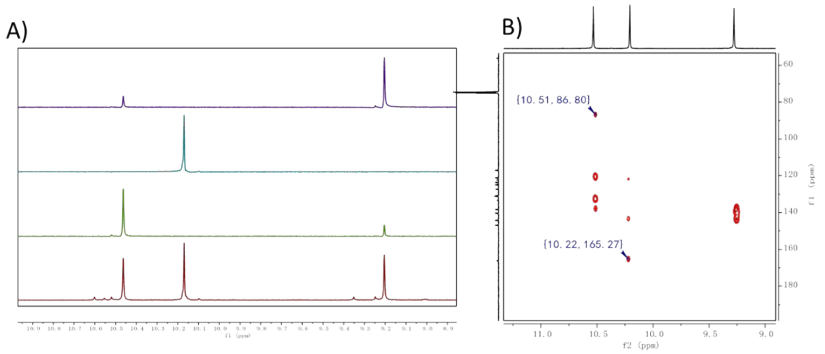

Figure S36. Aromatic region of 1D NOE (A) and HMBC (B) of **11**.

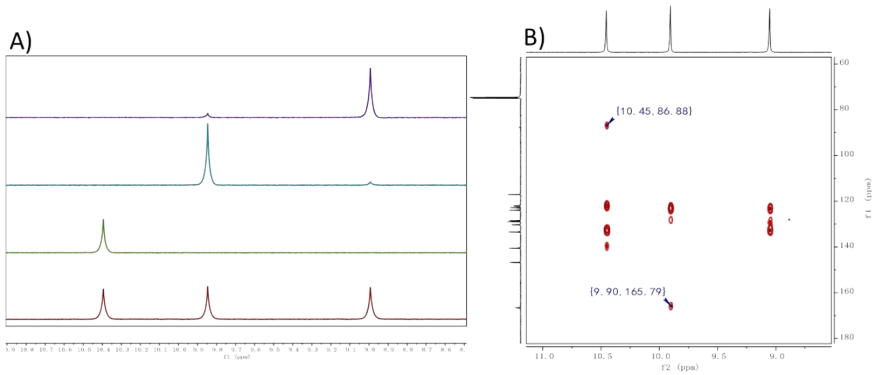

Figure S37. Aromatic region of 1D NOE (A) and HMBC (B) of **13**.